

Ensemble Quadratic Assignment Network for Graph Matching

Haoru Tan^{1,2} · Chuang Wang^{1,2,✉} · Sitong Wu² · Xu-Yao Zhang^{1,2} · Fei Yin^{1,2} ·
Cheng-Lin Liu^{1,2}

Received: date / Accepted: date

Abstract Graph matching is a commonly used technique in computer vision and pattern recognition. Recent data-driven approaches have improved the graph matching accuracy remarkably, whereas some traditional algorithm-based methods are more robust to feature noises, outlier nodes, and global transformation (e.g. rotation). In this paper, we propose a graph neural network (GNN) based approach to combine the advantage of data-driven and traditional methods. In the GNN framework, we transform traditional graph matching solvers as single-channel GNNs on the association graph and extend the single-channel architecture to the multi-channel network. The proposed model can be seen as an ensemble method that fuses multiple algorithms at every iteration. Instead of averaging the estimates at the end of the ensemble, in our approach, the independent iterations of the ensembled algorithms exchange their information after each iteration via a 1x1 channel-wise convolution layer. Experiments show that our model improves the performance of traditional algorithms significantly. In addition, we propose a random sampling strategy to reduce the computational complexity and GPU memory usage, so that the model is applicable to matching graphs with thousands of nodes. We evaluate the performance of our method on three tasks: geometric graph matching, semantic feature matching, and few-shot 3D shape classification. The proposed model performs comparably or outperforms the best existing GNN-based methods.

Keywords Graph Matching · Combinatorial Optimization · Graph Neural network · Ensemble Learning

¹National Laboratory of Pattern Recognition, Institute of Automation of Chinese Academy of Sciences, Beijing 100190, China

²School of Artificial Intelligence, University of Chinese Academy of Sciences, Beijing 100044, China

✉ Corresponding author: Chuang Wang (chuang.wang@nlpr.ia.ac.cn)

1 Introduction

Graph matching (GM) is a fundamental technique in computer vision, widely used in object recognition [83, 80], tracking [27, 13, 73], and shape matching [3, 38, 8] tasks. Given two graphs with certain node features, e.g. locations of feature points [89], GM aims to find the correspondence between the two sets of nodes, which is a typical combinatorial optimization problem.

In traditional algorithm-based approaches, GM is usually decomposed into two stages: modeling and optimization. At the modeling stage, the node features and graph structures are used to construct an affinity matrix, which measures the similarity of the nodes and edges from the two graphs. At the optimization stage, GM is formulated as a quadratic assignment problem (QAP) to find a 0-1 assignment vector that maximizes the sum of the affinity scores of all matched nodes and edges. Since QAP is an NP-hard problem, researchers developed a variety of relaxation strategies for efficiently approximating the solution of this optimization problem [48, 75, 84].

Recently, benefiting from the deep learning technology, a series of data-driven approaches have been proposed to treat the two steps of feature representation learning and combinatorial optimization jointly [63, 76, 53, 51, 89, 74, 64], and have achieved remarkable improvement in matching accuracy on several public datasets. The improvements largely owe to learning better feature representations, while the optimization solver is mostly akin to the traditional algorithms [5, 23, 43, 53, 77]. The integration of the optimization solver into an end-to-end trainable model is done by transforming the affinity matrix into a differentiable map. For example, the power method for solving the leading eigenvector of the affinity matrix corresponds to the recent work, GMN [5], and the proximal method for solving a relaxed QAP problem relates to the proximal matching neural network [23]. Further, Ro-

linek et al. [53] showed that many other traditional methods can also be used to build a black-box neural network for graph matching.

The data-driven models, despite their high prediction accuracy of node correspondence on given datasets, often suffer from data distribution shifts [89], e.g., random rotation. On the contrary, traditional methods are more robust to data transformations and noises.

In this paper, we propose an ensemble quadratic assignment network (EQAN) that combines the advantages of both the traditional and data-driven methods. Our model is constructed based on an observation that a traditional algorithm corresponds to a single-channel GNN model on an association graph, which is the Cartesian product of the two input graphs, and therefore a multi-channel GNN on the association graph relates to an ensemble of multiple base solvers. Instead of naive average of the multiple independent algorithms at the end of the iterations, in our approach, the base solvers exchange their information right after each iteration via a 1×1 channel-wise convolution layer. Moreover, we introduce an affinity update scheme to further boost the matching accuracy. Experiments show that the proposed model improves traditional methods dramatically, whereas the naive ensemble method does not yield noticeable change.

In addition, to handle large graphs with thousands of nodes, we present a random sampling strategy, which reduces the GPU memory footprint and the theoretical computational complexity of EQAN. Experiments show that the random sampling strategy improves the scalability of EQAN dramatically without significant performance loss. This strategy allows us to apply the proposed method to applications requiring a huge number of nodes, for example, few-shot 3D shape classification.

We evaluate the performance of our method on three tasks: geometric graph matching, semantic feature matching, and few-shot 3D shape classification. The proposed model performs comparably or outperforms the best existing GNN-based methods.

This work is built up on our conference paper [23] with extensively improvement and new contributions. In [23], we developed a differentiable proximal matching (DPGM) network for graph matching based on the proximal optimization method, which can be considered as a single-channel GNN. In this work, we design a multi-channel deep ensemble network, where each channel is a single-channel QAP-solver, e.g., proximal optimizer. However, the base matching solver is not limited to the proximal method. Other traditional methods, for example, the spectrum method [48], the graduated assignment method [72] and the re-weighted random walk matching (RRWM) [54], can also be integrated into the proposed framework, and gain a significant performance improvement as well. Experiments show that we achieved an improvement of approximately 5.6 percent on geometric

graph matching tasks and 13.0 percent on semantic feature matching tasks compared with our previous work [23].

The main contributions of this paper are summarized as follows.

- We introduce the ensemble quadratic assignment network (EQAN) for solving graph matching problems. It combines the advantages of traditional and data-driven methods to enhance both matching accuracy and robustness.
- We proposed a random sampling strategy to improve the scalability so that our method can fit problems with thousands of nodes.
- Experiments on three computer vision tasks, geometric graph matching, semantic feature matching, and few-shot 3D shape classification, reveal the good performance of our model.

The remaining paper is organized as follows. Section 2 reviews related works. Section 3 introduces the graph matching task and differentiable solvers. Section 4 describes our ensemble framework. Section 5 formulates our method as a multi-channel graph neural network, and introduces the affinity update scheme to boost the performance and the random sampling strategy for better scalability. Section 6 presents the experimental results, and Section 7 draws concluding remarks.

2 Related Works

2.1 Traditional graph matching algorithms

Traditional works developed varieties of relaxation and approximated optimization strategies for solving the optimization problem of graph matching (GM) tasks. A series of GM algorithms [48, 78, 25, 46] were built based on the spectral technique. They converted the GM problem to the task of finding the leading eigenvector of the affinity matrix. GAGM [72] uses a gradient-based graduated assignment technique under the bi-stochastic relaxation technique (also known as the doubly stochastic relaxation). This relaxation replaces the space of permutation matrices with the space of doubly stochastic matrices. RRWM [54] is a random-walk-based method that transforms the GM into the problem of selecting reliable nodes from the association graph. IPFP [42] directly computes the solution in the discrete assignment space without the continuous-variable relaxation.

Usually, the plain implementations of the GM algorithm have high computational complexity. A line of works aims to improve the scalability by avoiding maintaining the complete affinity matrix. For instance, FGM [17] decomposes the affinity matrix into smaller blocks and introduces global geometric constraints. KerGM [90] provides a unified perspective for Koopmans-Beckmann’s and Lawler’s QAP by

introducing new rules for array operations in the associated Hilbert spaces. Wang et al. [19] proposed a functional representation for graph matching to avoid computing the affinity matrix.

The traditional approaches primarily focus on developing better and faster algorithms for solving the underlying optimization problem. In those works, the graph features and affinity matrix are mostly hand-crafted. In practice, seeking a good representation of node features greatly affects the performance [5].

2.2 Data-driven graph matching models

Depending on the training data type and the input feature, we roughly classify the existing data-driven methods into two types. The first type focuses on visual feature matching [51, 63, 5, 53, 88], in which pixels information are available and the models usually incorporate a deep convolutional neural network (CNN), *e.g.*, VGG [39] for feature encoding. The second type is referred to as geometric matching, where only the locations of nodes are given. In this case, a graph neural network (GNN) [89, 51, 11, 23] is deployed to generate high-order features by aggregating local geometric information. Other methods [51, 74] are applicable to both situations.

Recent data-driven approaches combine feature extractor and optimization solver in a unified model and train the model in an end-to-end fashion. Wang et al. [63] proposed a differentiable deep network pipeline for learning soft permutation and graph embedding. Yu et al. [76] proposed a deep graph matching learning method with channel-independent embedding (CIE) and Hungarian attention. The above GM algorithms involve the Hungarian method to discretize the continuous solution, in which the discretization procedure cuts off the end-to-end computational graph, Rolínek et al. [53] addressed this challenge by estimating the gradient flow of the matching algorithm in a black-box manner. Fey et al. [51] proposed a two-stage graph neural matching method, called deep graph matching consensus (DGMC), that achieves remarkable performance by incorporating a local consensus requirement. Gao et al. [59] presented a deep learning framework that explicitly formulates pairwise graph structures as a quadratic constraint. Zeng et al. [68] proposed a parameterized graph matching framework by linearly combining multiple Koopmans–Beckmann’s graph matchings. Liu et al. [10] proposed a reinforcement learning approach for sequentially finding the node-to-node matching. Liu et al. [43] proposed a stochastic iterative graph matching model (SIGMA) by defining a distribution of matchings for the input graph pair. Yu et al. [77] proposed a deep latent graph matching model (DLGM) to learn the matching results and the latent topology of the input graph jointly.

A few works have involved the association graph for graph matching [54, 74, 64]. Cho et al. [54] showed that com-

puting the node-wise correspondence is equivalent to picking trustworthy nodes from the association graph. Wang et al. [74] proposed a novel neural combinatorial optimization solver on the association graph, which seeks to learn affinity and solvers simultaneously. Wang et al. [64] expands the GNN solver (NGM) on the association graph applicable to more broad QAP problems.

On data utilization, the deep graphical feature learning (DGFL) method [89] introduced the synthetically supervised pipeline, in which the model is trained with only synthetic random graphs and is tested on real-world datasets. Wang et al. [66] presented an unsupervised graph matching technique that simultaneously learns graph clustering and graph matching.

Though existing GNN-based approaches have achieved remarkable improvement in term of matching accuracy on several public datasets, they are usually not robust to data transformations and noises [89] as traditional optimization-based methods [23]. Figure 5 demonstrates a concrete comparative experiment. The proposed EQAN not only inherits the good robustness of traditional methods but also maintains the high accuracy of deep GM methods via mapping an ensemble of several base solvers (not limited to our DPGM) as a multi-channel GNN with additional designation on how to share information among channels and how to utilize the affinity matrix.

2.3 Applications

The surveys [36, 57, 47] reviewed application scenarios of graph matching methods. Here are some typical examples of computer vision and pattern recognition. Shen et al. [16] applied graph matching tools to medical image registration. Wu et al. [86] presented a novel graph matching approach for remote sensing image registration. Nie et al. [82] and He et al. [31] use graph matching tools to solve the problem of object tracking. Shen et al. [85], Wang et al. [26], and Zhao et al. [33] proposed using graph matching methods to tackle the person re-identification problem. Wang et al. [1] proposed a scene-understanding approach based on graph matching. Liao et al. [12] and Zhang et al. [90] applied graph matching methods to the problem of aligning multiple protein networks. Fiori et al. [45] used graph matching algorithms to infer brain connectivity from functional magnetic resonance imaging data. He et al. [29] proposed a GM-based approach to find the semantic correspondences between images. Justin et al. [70] and Fu et al. [40] used graph matching tools to analyze 3D CAD models and point clouds. Chopin et al. [28] reformulated image segmentation as an inexact graph-matching problem with many-to-one constraints. In addition to these, many practical tasks, such as action recognition [6], visual localization [20], real-time matching of image wireframes [34], pose estimation [44],

etc., also need to estimate the point-to-point correspondence between multiple images.

In all these applications, high matching accuracy and efficiency (scalability to large graphs) are always desirable.

3 Graph Matching and Differentiable Solver

3.1 Problem formulation

Graph matching aims to find the correspondence of nodes between two graphs. Let $G_1 = (V_1, E_1)$ and $G_2 = (V_2, E_2)$ be two undirected graphs. We assume that the graphs have an equal number of nodes $|V_1| = |V_2| = n$. For the unequal case, one can always add additional dummy nodes to meet this condition.

Formally, graph matching can be formulated as a quadratic assignment problem (QAP) [48]

$$\max_{\mathbf{x} \in \{0,1\}^{n^2}} \mathbf{x}^\top \mathbf{M} \mathbf{x} \quad \text{s.t.} \quad \mathbf{C} \mathbf{x} = \mathbf{1}, \quad (1)$$

where \mathbf{x} is an assignment vector such that $[\mathbf{x}]_{ij} = 1$ if node i in G_1 corresponds to node j in G_2 , and 0 otherwise; the affinity matrix $\mathbf{M} \in \mathcal{R}_+^{n^2 \times n^2}$ measures the similarity between the nodes in the two graphs; the binary matrix \mathbf{C} encodes $2n$ linear constraints: $\sum_{i \in V_1} [\mathbf{x}]_{ij'} = \sum_{j \in V_2} [\mathbf{x}]_{ij'} = 1$ for all $i' \in V_1$ and $j' \in V_2$. These constraints ensure that the matching map induced by any valid \mathbf{x} is bijective from V_1 to V_2 .

The affinity matrix is constructed based on the topology of the graphs and the local features associated with the nodes and edges. The diagonal terms $[\mathbf{M}]_{ii,jj}$ represents the reward if node i in G_1 is mapped to node j in G_2 . The off-diagonal terms $[\mathbf{M}]_{ii',jj'}$ represents the reward if a pair of nodes (i, i') in G_1 corresponds to a pair (j, j') in G_2 . A classical example is Koopman-Beckmann's construction $\mathbf{M} = \mathbf{A}_1 \otimes \mathbf{A}_2$ [79], where \mathbf{A}_1 and \mathbf{A}_2 are adjacent matrices of G_1 and G_2 respectively. Intuitively, $[\mathbf{M}]_{ii',jj'} = 1$ if and only if both pairs of (i, i') and (j, j') are directly connected in G_1 and G_2 respectively, and 0 otherwise.

3.2 Differentiable proximal graph matching

We introduce a classical algorithm to solve (1) approximately based on the proximal method [56]. In general, the integer optimization problem (1) is hard to solve. First, we relax it to a continuous optimization problem

$$\min_{\mathbf{z} \in \mathcal{R}_+^{n^2}} \mathcal{L}(\mathbf{z}) = -\mathbf{z}^\top \mathbf{M} \mathbf{z} - h(\mathbf{z}) \quad \text{s.t.} \quad \mathbf{C} \mathbf{z} = \mathbf{1}, \quad (2)$$

where $h(\mathbf{z}) = -\lambda \mathbf{z}^\top \log(\mathbf{z})$ is an entropy regularizer with the scalar λ being the regularizer parameter. The matrix \mathbf{C}

Algorithm 1 : Differentiable Proximal Graph Matching

Input: Affinity matrix \mathbf{M} , maximum iteration K and stepsize β .

Initialization: $\mathbf{z}_0 \leftarrow \text{Sinkhorn}(\mathbf{u})$.

for $k = 1$ **to** K **do**

$$\tilde{\mathbf{z}}_k \leftarrow \exp \left[\frac{\beta}{1+\lambda\beta} (\mathbf{M} \mathbf{x}_{k-1}) + \frac{1}{1+\lambda\beta} \log(\mathbf{z}_{k-1}) \right]$$

$$\mathbf{z}_k \leftarrow \text{Sinkhorn}(\tilde{\mathbf{z}}_k)$$

end for

Output \mathbf{z}_K

Algorithm 2 : Sinkhorn Method

Input: $\mathbf{X} \in \mathcal{R}_+^{n \times n}$, $T = 5$.

Initialization: $\mathbf{b} \leftarrow \mathbf{1}$, $\mu \leftarrow \mathbf{1}^{n \times 1}$, $\mathbf{v} \leftarrow \mathbf{1}^{n \times 1}$.

for $t = 0$ **to** $T - 1$ **do**

$$\mathbf{a} \leftarrow \frac{\mu}{\mathbf{X} \mathbf{b}}, \mathbf{b} \leftarrow \frac{\mathbf{v}}{\mathbf{X}^\top \mathbf{a}}.$$

end for

$$\mathbf{Y} = \text{Diag}(\mathbf{a}) \mathbf{X} \text{Diag}(\mathbf{b})$$

Output: \mathbf{Y}

is the same as the one in (1). The parameter λ controls the hardness of the optimization problem (2).

Then, we decompose the non-convex objective (2) into a sequence of convex sub-problems

$$\mathbf{z}_{t+1} = \underset{\mathbf{z} \in \mathcal{R}_+^{n^2 \times 1}, \mathbf{C} \mathbf{z} = \mathbf{1}}{\text{argmin}} \quad \mathbf{z}^\top \nabla g(\mathbf{z}_t) - h(\mathbf{z}) + \frac{1}{\beta} D(\mathbf{z}, \mathbf{z}_t) \quad (3)$$

where $g(\mathbf{z}) = -\mathbf{z}^\top \mathbf{M} \mathbf{z}$; the function $D(\cdot, \cdot)$ is a non-negative proximal operator with $D(\mathbf{x}, \mathbf{y}) = 0$ if and only if $\mathbf{x} = \mathbf{y}$; and $\beta > 0$ is a scalar parameter controlling the proximal weight. Since $[\mathbf{z}]_{ij} \in [0, 1]$, we can interpret it as the probability of mapping node i in G_1 to node j in G_2 . We choose the Kullback-Leibler divergence as the proximal function, i.e., $D(\mathbf{z}, \tilde{\mathbf{z}}) = \mathbf{z}^\top \log(\mathbf{z}) - \mathbf{z}^\top \log(\tilde{\mathbf{z}})$.

The convex optimization (3) has an analytical solution

$$\tilde{\mathbf{z}}_{t+1} = \exp \left[w_p \mathbf{M} \mathbf{z}_t + w_z \log(\mathbf{z}_t) \right], \quad (4)$$

$$\mathbf{z}_{t+1} = \text{Sinkhorn}(\tilde{\mathbf{z}}_{t+1}), \quad (5)$$

where $w_p = \frac{\beta}{1+\lambda\beta}$, $w_z = \frac{1}{1+\lambda\beta}$, and $\text{Sinkhorn}(\cdot)$ is the Sinkhorn-Knopp transform. The proof of convergence of the above DPGM algorithm and the detailed derivation of (4), (5) from (3) are presented in Appendix A.2 and A.3 respectively. Pseudo-codes are shown in Algorithm 1 and Algorithm 2. When applying the Sinkhorn-Knopp transform, we reshape the input (output) as a $n \times n$ matrix (n^2 -dimensional vector) respectively. One can check that (4) solves (3) ignoring the constraint $\mathbf{C} \mathbf{z} = \mathbf{1}$, and the normalization step (5) ensures that $\text{mat}(\mathbf{z}_{t+1})$ is a $n \times n$ doubly stochastic matrix.

3.3 General differentiable iterative solver

The proximal method introduced above is one of a large set of classical algorithms for solving the quadratic assignment

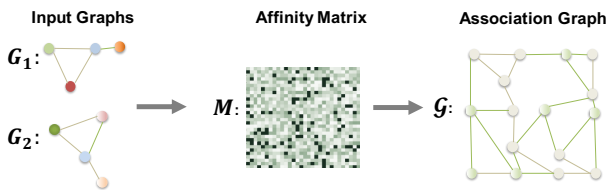


Fig. 1 The association graph $\mathcal{G} = (\mathcal{V}, \mathcal{E})$ of two base graphs $G_1 = (V_1, E_1)$ and $G_2 = (V_2, E_2)$. Each association-node from the association graph represents a candidate matching between a pair of nodes from two base graphs. Graph matching is equivalent to selecting a set of nodes in the association graph [54, 74, 64] with certain exclusive constraints.

problem (QAP) (1). Other methods are, for example, the spectrum method (SM) [5], and the graduated assignment graph matching (GAGM) algorithm [72]. The iteration equation of all these methods can be abstracted as a single transform

$$z_{t+1} = \text{QAP-Solver}(z_t, M; w_t), \quad (6)$$

where w_t encloses all algorithmic parameters at step t . In the proximal method (4), (5), the parameters are $w_t = [w_p, w_z]$. The spectrum method is a power iteration for solving the eigenvector of the leading eigenvalue of the affinity matrix, i.e., $z_{t+1} = Mz_t / \|Mz_t\|$. We listed the details of SM and GAGM methods in Appendix B.

Recent data-driven approaches [5, 23, 53] are based on an observation that the update transforms (6) is a differentiable map from M and z_t to z_{t+1} . Therefore, one can integrate the graph matching algorithm into a deep-learning framework by combing the feature extractor and the matching algorithm together and training them in an end-to-end manner. For example, GMN [5] used the spectrum method; our previous work [23], DPGM deployed the proximal method; and BBGM [53] considered (6) as a general black-box solver.

3.4 QAP-Solver as a single-channel GNN

In what follows, we show that a differentiable QAP-solver can be considered as a single-channel GNN on an association graph of two base graphs $G_1 = (V_1, E_1)$ and $G_2 = (V_2, E_2)$.

The association graph $\mathcal{G} = (\mathcal{V}, \mathcal{E})$, with an example shown in Figure 1, is constructed as follows. The association-node set \mathcal{V} is the Cartesian product of the two base node sets, i.e., $\mathcal{V} = V_1 \otimes V_2 = \{ij | i \in V_1, j \in V_2\}$. Each association-node indexed by the tuple ij from the association graph represents a candidate matching between a pair of nodes $\{i \in V_1, j \in V_2\}$ from two base graphs. The association-nodes ij and $i'j'$ from the association graph are connected if and only if (i, i') and (j, j') are edges in E_1 and E_2 .

To illustrate the connection between a QAP-solver and GNN, we take the DPGM method (4), (5) as a concrete example. In particular, the matrix multiplication Mz_t in (4)

can be decomposed into two neural message passing steps [67]: the aggregation step and the local update step

$$\begin{aligned} [\tilde{z}_{t+1}]_{ij} = \exp & \left[\underbrace{w_p \sum_{i'j' \in \mathcal{N}_{ij}} [M]_{ii',jj'} [z_t]_{i'j'}}_{\text{aggregation}} \right. \\ & \left. + \underbrace{w_p [M]_{ii,jj} [z_t]_{ij}}_{\text{local update}} + \underbrace{w_z \log([z_t]_{ij})}_{\text{Damping}} \right]. \end{aligned} \quad (7)$$

In the aggregation step, the pairwise affinity $[M]_{ii',jj'}$ is the weight to aggregate the neighbor's message $[z_t]_{i'j'}$ to the central association-node ij . In the local update step, the central association-node ij update its previous value $[z_t]_{ij}$ according to the unary potential $[M]_{ii,jj}$. The exponential function acts as the nonlinear activation unit and w_p is used as the transformation parameter during message passing. Then, the Sinkhorn operation (5) normalizes \tilde{z}_{t+1} and produces the output z_{t+1} .

The ij th association-node message $[z_t]_{ij}$ in the above message passing rule is a scalar. Therefore, the corresponding GNN only has a single channel, which usually has a limited capacity for modeling complex relationships. Nevertheless, this analogy motivates us to develop a multi-channel GNN on the same association graph resulting in the proposed ensemble model, in which the feature of the ij th association-node is generated by fusing the corresponding association-node messages from multiple QAP-solvers (single-channel GNNs). Details are illustrated in the following two sections.

4 Ensemble Quadratic Assignment Model

As depicted in Figure 2, the proposed ensemble quadratic assignment model consists of three sequential modules. First, the *initialization module* constructs initial node features from raw inputs. Then, the *ensemble assignment module* refines the node features using a sequence of ensemble blocks. Each block is a set of QAP-solvers. Finally, the *decision layer* generates the final matching score and prediction from the refined features.

4.1 Initialization module

The initialization module aims to construct the affinity matrix M and initialize a feature tensor $V^{(0)}$ from the raw inputs, e.g. location of nodes and local pixel values. This module can be formulated as

$$V^{(0)}, M = \text{Initialization-Module}(G_1, G_2), \quad (8)$$

where G_1 and G_2 contain the raw node features and graph structures of input graphs respectively. Inside this module, firstly, we convert the raw input features associated with the

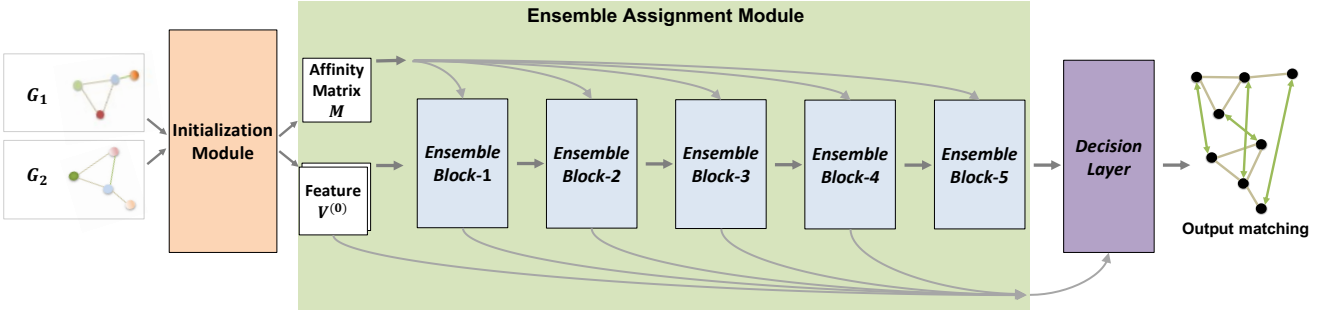


Fig. 2 The ensemble quadratic assignment model consists of three modules. The initialization module computes the affinity matrix and initializes the iteration feature tensor. The ensemble assignment module is a sequence of ensemble blocks, which include a set of classical QAP solvers. Details are shown in Figure 3. The final layer takes the features created by all previous blocks as input and outputs a matching decision.

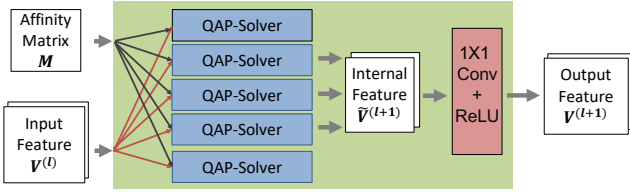


Fig. 3 An *Ensemble Block* includes a set of QAP-solvers that update the channels of feature independently, and a 1×1 convolution layer that promotes information exchange across the channels.

nodes of each graph into a set of d -dimensional vectors denoted by $\mathbf{F}_q \in \mathcal{R}^{n \times d}$, $q = 1, 2$. A vanilla implementation is simply concatenating all raw information with proper value scaling. A better but optional method is employing a graph neural network (GNN) to extract local features by aggregating a certain range of neighbor information [89, 51, 63].

Then, we construct the affinity matrix \mathbf{M} by setting the diagonal terms $[\mathbf{M}]_{ii,jj} = \|[\mathbf{F}_1]_{i,:} - [\mathbf{F}_2]_{j,:}\|$, and the off-diagonal terms

$$[\mathbf{M}]_{ii',jj'} = \begin{cases} e^{-|d_{ii'}^{(1)} - d_{jj'}^{(2)}|^2 / \sigma^2}, & \text{if } (i, i') \in G_1, (j, j') \in G_2, \\ 0, & \text{otherwise,} \end{cases}$$

where $d_{ii'}^{(1)} = \|[\mathbf{F}_1]_{i,:} - [\mathbf{F}_1]_{i',:}\|$ and $d_{jj'}^{(2)} = \|[\mathbf{F}_2]_{j,:} - [\mathbf{F}_2]_{j',:}\|$, and σ is a (predefined or learnable) parameter.

Lastly, we initialize the multi-channel feature tensor $\mathbf{V}^{(0)}$ by concatenating the raw features and performing a channel-wise linear transform. Specifically, the operation is

$$[\hat{\mathbf{V}}]_{:,i,j} = \text{Concate}\left(\|[\mathbf{F}_1]_{i,:} - [\mathbf{F}_2]_{j,:}\|, [\mathbf{F}_1]_{i,:}, [\mathbf{F}_2]_{j,:}\right), \quad (9)$$

$$\mathbf{V}^{(0)} = \text{ReLU}\left(\text{Conv-}1 \times 1(\hat{\mathbf{V}})\right), \quad (10)$$

where $|\cdot|$ is the entry-wise absolute operation, and the operation $\text{Conv-}1 \times 1(\hat{\mathbf{V}})$ is the 1×1 convolutional operation mapping from $\mathcal{R}^{(3d) \times n \times n}$ to $\mathcal{R}^{C \times n \times n}$ by performing a linear transform along $\hat{\mathbf{V}}$'s first coordinate axis (enumerating the indices of the second and third axes).

4.2 Ensemble assignment module

The ensemble assignment module refines the feature tensor $\mathbf{V}^{(\ell)}$ iteratively, $\ell = 1, 2, \dots, L$. Formally, we write

$$\mathbf{V}^{(\ell)} = \text{EnsembleBlock}^{(\ell)}\left(\mathbf{V}^{(\ell-1)}; \mathbf{M}\right), \quad (11)$$

with the initial feature tensor $\mathbf{V}^{(0)}$ and \mathbf{M} received from the initialization module. In this module, all *EnsembleBlock* use the same affinity matrix \mathbf{M} .

The *EnsembleBlock* consists of a set of parallel QAP solvers (12) and a 1×1 convolution layer. We draw its detailed structure in Figure 3. The QAP-solvers update the feature tensors channel-by-channel independently as a QAP layer, *i.e.*

$$[\tilde{\mathbf{V}}^{(\ell)}]_{c,:} = \text{QAP-Layer}\left([\mathbf{V}^{(\ell-1)}]_{c,:} + \epsilon, \mathbf{M}; \mathbf{w}^{(\ell,c)}\right), \quad (12)$$

where $[\mathbf{V}^{(\ell-1)}]_{c,:} \in \mathcal{R}^{n \times n}$ is the slice of the feature tensor with a given channel c ; $\mathbf{w}^{(\ell,c)}$ is the internal parameters inside the solver; ϵ is a very small number set as 10^{-5} to avoid the error, $\log 0 = -\text{inf}$, when $\text{ReLU} = 0$ in (10) and (13). The QAP-Layer can be any classical matching algorithm, as long as the corresponding map is differentiable.

After the channel-wise update, we use the 1×1 convolution layer to exchange information of $\tilde{\mathbf{V}}$ among channels

$$\mathbf{V}^{(\ell)} = \text{ReLU}\left[\text{Conv-}1 \times 1(\tilde{\mathbf{V}}^{(\ell)})\right]. \quad (13)$$

By combining (12) and (13), we build the update equation (11) for a single *EnsembleBlock*.

Finally, after L iterations of (11), we concatenate all feature tensors $\{\mathbf{V}^{(\ell)}\}$ as the output of this module,

$$\mathbf{V} = \text{Concate}([\mathbf{V}^{(0)}, \dots, \mathbf{V}^{(L)}]) \in \mathcal{R}^{(L+1)C \times n \times n}. \quad (14)$$

Experiments show that fusing of all feature tensors performs better than only using the last one.

4.3 The decision layer

The decision layer maps the global feature \mathbf{V} defined in (14) to a reward matrix $\mathbf{R} \in \mathcal{R}_+^{n \times n}$ via

$$\mathbf{R} = \exp \left(\text{Conv-}1 \times 1(\mathbf{V}) \right), \quad (15)$$

where the 1×1 convolutional operation performs the linear transform along \mathbf{V} 's first coordinate axis. The entry $[\mathbf{R}]_{ij}$ is a positive reward of matching node i in G_1 with node j in G_2 . Then, we normalize \mathbf{R} by

$$\mathbf{Q} = \text{Sinkhorn}(\mathbf{R}) \quad (16)$$

and get a non-negative soft matching prediction matrix \mathbf{Q} . The entry $[\mathbf{Q}]_{ij}$ can be interpreted as the estimated probability that node i in G_1 matches node j in G_2 .

In the training phase, we use the cross entropy loss [63] to calculate the loss between the prediction matrix \mathbf{Q} and the ground-truth assignment \mathbf{x}^* ,

$$L(\mathbf{Q}, \mathbf{x}^*) = -\langle \mathbf{x}^*, \log \mathbf{Q} \rangle - \langle 1 - \mathbf{x}^*, \log(1 - \mathbf{Q}) \rangle, \quad (17)$$

where $\langle \cdot, \cdot \rangle$ refers to the inner product operation for clarity.

At the testing stage, we deploy the Hungarian method [24] to get 0-1 decision variable from the matrix \mathbf{Q} . The Hungarian method is widely adopted for linear programming problems [42, 63, 5, 51, 89], with $\mathcal{O}(n^3)$ complexity, where n is the node number of the input graph. Note that even though the Hungarian method consumes the highest complexity in our model, it takes less than 0.6 seconds when the input graphs are of size $n = 1000$. We find that the real obstacle on the scalability of the model is the large memory footprint caused by the large matrix multiplication, see Section 5.3.

5 Ensemble model as a graph neural network

In this section, we interpret our ensemble quadratic assignment model as a graph neural network (GNN) based on the observation in Sec.3.3 that the QAP-solver can be considered as a single-channel GNN on an association graph. We first connect the ensemble model to the multi-channel GNN and discuss the difference from the conventional GNN models. Then, we propose an affinity update scheme to enhance the matching performance, and then introduce a random sampling strategy to reduce both the computational complexity and the GPU memory footprint to make our model suitable for large-scale problems. Finally, we analyze the computational complexity.

5.1 Ensemble model is a multi-channel GNN

In the ensemble model, multiple channels are updated in parallel as in (11). This can be seen as a multi-channel extension of (7).

Different from the conventional GNN models, where the convolution kernel \mathbf{M} is a learnable matrix, we consider \mathbf{M} as another input variable. For the graph matching problem, \mathbf{M} encloses the node affinity between two base graphs, which heavily depends on the input information and varies instance by instance. Therefore, we design the specialized GNN architecture shown in Figure 2. The kernel \mathbf{M} is computed by the initialization module defined in (8), see Section 4.1. All the ensemble blocks share the same kernel. Under this structure, given \mathbf{M} , each channel of node features evolves independently. To promote information exchange among channels, we append a 1×1 convolution layer, of which the 1×1 kernel is a learnable parameter. By this design, our ensemble model inherits the high flexibility of GNNs and meanwhile utilizes the effectiveness of the classical graph matching algorithms.

5.2 Affinity update scheme

In the ensemble model described above, the convolution kernel \mathbf{M} is shared among various modules, which limits the representational ability of the model to some extent. Based on the GNN properties, we design an affinity update scheme to improve this situation.

Specifically, the pair-wise and node-wise affinity is updated according to

$$\begin{aligned} \mathbf{M}_{ii',jj'}^{(\ell)} &= \exp \left[-\mathbf{w}^{(\ell)\top} \left(\mathbf{V}_{:,i,j}^{(\ell)} - \mathbf{V}_{:,i',j'}^{(\ell)} \right)^2 \right], \\ \mathbf{M}_{ii,jj}^{(\ell)} &= \exp \left[\mathbf{u}^{(\ell)\top} \mathbf{V}_{:,i,j}^{(\ell)} \right], \end{aligned} \quad (18)$$

where $\mathbf{w}^{(\ell)}$ and $\mathbf{u}^{(\ell)}$ are two learnable parameter vectors, $\mathbf{V}_{:,i,j}^{(\ell)}$ is the representation of the ij th association-node from the association graph, and the square in the first equation is an element-wise operation. Intuitively, the two learnable parameters $\mathbf{w}^{(\ell)}$ and $\mathbf{u}^{(\ell)}$ controls the weight on how much different channels of the association-node features contributes to the pair-wise and node-wise affinity in the next layer. Thus, the inference rule in (11) of the EnsembleBlock should be modified to

$$\mathbf{V}^{(\ell)}, \mathbf{M}^{(\ell)} = \text{EnsembleBlock}^{(\ell)} \left(\mathbf{V}^{(\ell-1)} ; \mathbf{M}^{(\ell-1)} \right),$$

where each block indexed by $\ell \in \{2, \dots, L\}$ takes the feature tensor $\mathbf{V}^{(\ell-1)}$ and the updated affinity matrix $\mathbf{M}^{(\ell-1)}$ from the previous $(\ell - 1)$ th block as input. When $\ell = 1$, the input affinity matrix $\mathbf{M}^{(0)}$ is the initial affinity matrix from the initialization module, see Section 4.1.

5.3 Scaling to large graphs via random sampling

We present a random sampling strategy to make our model scalable to large graphs (those with as many as > 1000 nodes). The general idea is to approximate the iteration equation (4) by only updating a random subset of items and directly copying the remaining entries from its corresponding input entries. This technique not only lowers theoretical computational complexity but also reduces GPU memory consumption. Moreover, the performance does not vary significantly.

Specifically, we first generate a random mask $B_{c,i,j}^{(\ell)} \in \{0, 1\}$ with $q_{i,j}^{(\ell)}$ probability being 1 for each layer $\ell \in \{1, \dots, L\}$, channel c , and position i, j . Note that the random mask B is also not shared across different input data pairs. The probability is computed by

$$q_{i,j}^{(\ell)} = [\mathbf{S}^{(\ell)}]_{i,j} / \left(\sum_{k\bar{k}} [\mathbf{S}^{(\ell)}]_{k\bar{k}} \right),$$

where the sampling weight $[\mathbf{S}^{(\ell)}]_{i,j} = \frac{1}{C} \sum_{c=1}^C [\tilde{\mathbf{V}}^{(\ell-1)}]_{c,i,j}$ for $\ell > 1$, and $\tilde{\mathbf{V}}^{(\ell-1)}$ defined by (12) is the internal representations in the previous block, *e.g.*, the outputs of all solvers in the previous ensemble block. For the first block, $\ell = 1$, we set $[\mathbf{S}^{(1)}]_{i,j} = [\mathbf{M}]_{ii,jj}$, where \mathbf{M} is the affinity matrix generated from the initialization module.

Then, for each channel c , we modify the QAP-solver so that it only updates the corresponding $[\tilde{\mathbf{z}}]_{i,j}$ in (4) if $B_{c,i,j}^{(\ell)} = 1$, and copy the remaining entries from its input. Formally, we rewrite the update rule (4) to

$$\begin{aligned} [\tilde{\mathbf{z}}_{\ell+1}]_{i,j} &= B_{c,i,j}^{(\ell)} \left[\exp \left(w_p \mathbf{M} \mathbf{z}_\ell + w_z \log(\mathbf{z}_\ell) \right) \right]_{i,j} \\ &+ (1 - B_{c,i,j}^{(\ell)}) [\tilde{\mathbf{z}}_\ell]_{i,j}. \end{aligned} \quad (19)$$

The proposed sampling scheme is inspired by the neural network pruning [92,22], that the neurons with small-scale outputs and the connections with negligible weights are considered as uninformative, which can be pruned without significant impact on the performance.

Approximated backward propagation The above random sampling strategy introduces a non-differentiable path along sampling weight matrix $\mathbf{S}^{(\ell)}$ and the random mask $B_{c,i,j}^{(\ell)}$. We solve this issue by proposing an approximated backward propagation.

The weight matrix $\mathbf{S}^{(\ell)}$ affect the probability distribution of the random variable $B_{c,i,j}^{(\ell)}$ via $q_{i,j}^{(\ell)}$, but $B_{c,i,j}^{(\ell)}$ does not directly depends on $\mathbf{S}^{(\ell)}$. There is no explicit backward gradient path along those two variables. It introduces a non-differentiable path along sampling weight matrix $\mathbf{S}^{(\ell)}$ and the random mask $B_{c,i,j}^{(\ell)}$. We solve this issue by using the straight-through estimator (STE) to approximate the gradient

[7]. Specifically, STE approximates the gradient $\frac{\partial L}{\partial \mathbf{S}_{i,j}^{(\ell)}} = \sum_{c,t,k} \frac{\partial L}{\partial B_{c,t,k}^{(\ell)}} \frac{\partial B_{c,t,k}^{(\ell)}}{\partial q_{t,k}^{(\ell)}} \frac{\partial q_{t,k}^{(\ell)}}{\partial \mathbf{S}_{i,j}^{(\ell)}}$ by assuming $\frac{\partial}{\partial q_{i\bar{i}}^{(\ell)}} B_{c,i,j}^{(\ell)} \approx 1$.

Thus, we have

$$\begin{aligned} \frac{\partial L}{\partial \mathbf{S}_{i,j}^{(\ell)}} &\approx \sum_{c,t,k} \frac{\partial L}{\partial B_{c,t,k}^{(\ell)}} \frac{\partial q_{t,k}^{(\ell)}}{\partial q_{t,k}^{(\ell)}} \frac{\partial q_{t,k}^{(\ell)}}{\partial \mathbf{S}_{i,j}^{(\ell)}} \\ &= \frac{1}{\sum \mathbf{S}^{(\ell)}} \sum_{c,t,k} \frac{\partial L}{\partial B_{c,t,k}^{(\ell)}} (\delta_{t:i} \delta_{k:j} - q_{i,j}^{(\ell)}), \end{aligned} \quad (20)$$

where $\delta_{t:i}$ is the Dirac delta function that $\delta = 1$ when t equals i , and $\delta = 0$ otherwise.

The straight-through estimator (STE) [7] used above estimates the gradient via network quantization and network pruning. It considered back-propagating gradients through a piece-wise constant function that has zero gradients almost everywhere. The STE ignores the quantization (discretization) function in the backward pass and passes the gradient through as if it acts as an identity function. Yin et. al. [58] provides a theoretical justification of STE, which proved that the expected coarse gradient given by the STE-modified chain rule converges to a critical point of the population loss minimization problem.

5.4 Complexity analysis

The update rule (4), the most costly part of the overall complexity of the model, has the complexity $\mathcal{O}(K^2 n^2)$, where n is the size of the node set of the input graphs G_1 and G_2 , and K is the largest node degree in G_1 and G_2 . The dominating part is the matrix-vector product $\mathbf{M} \mathbf{z}_i$ in (4). In practice, we set the number of sampled entries in \mathbf{z} to be updated proportionally to $n\sqrt{n}$ in each QAP-solver, which is much less than the number of all entries n^2 in \mathbf{z} . Thus, the complexity of the update (4) is reduced to $\mathcal{O}(K^2 n\sqrt{n})$. In the view of graph neural network, this sampling operation is equivalent to using the message-passing mechanism to update the information of a few randomly selected association-nodes from the association graph. In Section 6.5.8, we further investigate practical running time at inference stage.

In addition, we note that the overall theoretical time complexity of the whole EQAN model is still $\mathcal{O}(n^2)$, which is dominated theoretically by the Sinkhorn normalization step and the final decision layer. On the other hand, the sampling scheme, as analyzed above, reduces the number of nodes to be updated from n^2 to $n\sqrt{n}$. The major target of this sampling strategy is to reduce the GPU memory footprint, which makes the model scales up to thousand of nodes in a single 12GB GPU card.

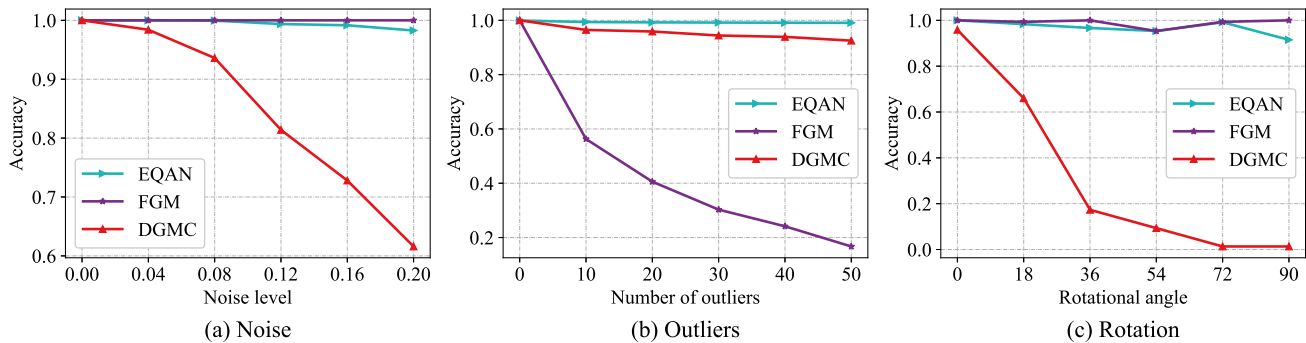


Fig. 4 Robustness to noise, outliers, and random rotation. (a) The noise level σ changes from 0.0 to 0.2, with $n_{in} = 50$, and $n_{out} = 0$. (b) We add a number of outliers n_{out} from 0 to 50 with $n_{in} = 35$, and $\sigma = 0.1$. (c) The maximum rotational angle ranges from 0 to 90 with $n_{in} = 30$, $n_{out} = 15$, and $\sigma = 0.1$.

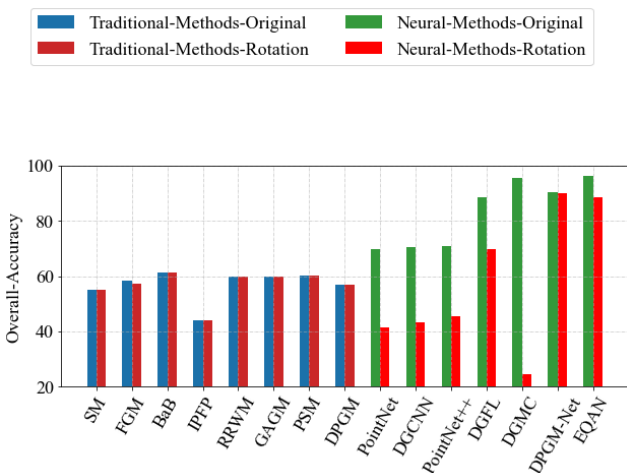


Fig. 5 Robustness of matching accuracy to random rotations. Left/right bar shows the accuracy on the original/rotated data respectively in each method. Traditional solvers is robust to global rotation but less accurate, whereas existing GNN methods improves the accuracy noticeably but they are very sensitive to global rotations. Our methods (DPGM-net and EQAN) inherit the advantages of both sides.

6 Experiments

We conducted a series of experiments to evaluate the performance of the proposed method. First, we test its robustness in three aspects: raw feature noise, outliers, and random rotation. Then, we compare the performance with existing methods in three tasks: geometric graph matching task, semantic feature matching, and few-shot 3D shape classification. Finally, we present ablation studies to investigate the effects of internal settings of our approach. All experiments were implemented in PyTorch [2] and run on a computer with the Intel Xeon E5-2680 processor and the NVIDIA TITAN GPU.

We use the proximal QAP-solver (DPGM) to construct the ensemble network. We implement three variants of our ensemble model, namely the naive ensemble quadratic assignment network (EQAN), the network with the affinity update scheme (EQAN-U) in Section 5.2, and the network

with the random sampling strategy (EQAN-R) in Section 5.3 respectively. The reported results of our methods in experiments are the average score of 5 independent runs (20 runs for few-shot 3D shape classification).

Training with synthetic data In the robustness test, the 2D geometric graph matching task, and the 3D-shape few-shot classification task, we train the model solely on the synthetic data [89]. This setting is more challenging to test generalization ability, and it is close to the practical situation when node-level annotated data is expensive or not available for training. In those experiments, we generate the reference graph G_1 with n_{in} inliers nodes embedded in a d -dimensional Euclidean space ($d = 2, 3$). The node feature information is uniformly drawn from $[-1, 1]^d$ and each node is connected to its top-5 nearest neighbors. Then, the query graph G_2 is generated by adding Gaussian noise to the nodes of a duplicated graph with zero mean and standard variance σ . In addition, we introduce n_{out} randomly uniform outlier nodes to G_2 .

Evaluation metric For geometric graph matching and semantic feature matching, we evaluate the matching accuracy by calculating the ratio of the number of correctly matched node pairs to the total number of ground truth node pairs [63]. For the few-shot shape classification, the classification accuracy is computed by calculating the ratio of the number of correctly classified query samples to the query set size [32, 61].

6.1 Robustness test

We test the sensitivity of our model to the feature noise, a number of outliers, and 2D rotations in the 2D graph matching setting, where the data generation settings of σ , n_{in} , n_{out} are listed in the caption of Figure 4. Experimental results are shown in Figure 4. We compare our method with the classical algorithm, FGM [17], and the GNN-based approach,

DGMC [51]. The affinity constructing of FGM is following the settings in [17]. The settings for DGMC are the same as the geometric graph matching settings in [51]. For our model, the block number in our model is $L = 5$, and each block consists of $C = 32$ proximal QAP-solvers [23]. In training, we use the Adam optimizer [14] with a learning rate of $1e-4$, batch size of 8, total iterations of 80000, and a warm-up stage of 500 iterations with a learning rate of $1e-10$.

In the first test of noise robustness, the classical algorithm FGM is stable against the noise and our approach’s performance drops slightly when increasing the noise, whereas the GNN-based method, DGMC is very sensitive to noise. In the second test of outlier robustness, the classical algorithm FGM deteriorates remarkably with outliers, while our approach and the DGMC work stably. In the third test of rotation sensitivity, the traditional algorithm FGM and our approach are almost unaffected to the rotation but the performance of DGMC drops remarkably.

In addition, we compare with other 14 peer methods including both types of traditional optimizer and GNN-based approaches in term of average matching accuracy under random rotations between 0 to 90 degrees. Results are shown in Figure 5. Similar experiments on Willow-Object dataset were reported in our conference work [23]. In general, traditional solvers is robust to global rotation but less accurate, whereas previous GNN methods improve the accuracy noticeably but they are very sensitive to global rotations.

The above results verify that our approach not only inherits the strong robustness of traditional algorithms but also preserves the high prediction accuracy of graph neural network methods.

6.2 Geometric graph matching

We compare the performance of geometric graph matching on the PASCAL-PF [55], which consists of 1351 image pairs within 20 classes. Each image pair contains 4-17 manually labeled ground-truth correspondences. This task aims to estimate the correspondence with only the coordinates of keypoints [89,51,17,54,90]. The experimental results are reported in Table 1.

We implemented the recently proposed data-driven approaches as baselines, including the DGFL [89], DGMC [51], Pointnet [11], and the DPGM-Net [23] which is an end-to-end network that utilizes the proximal solver with a graph neural network [89] to generate features for affinity matrix computing.

In geometric graph matching, our model directly uses the normalized coordinates as the input features F_1 and F_2 for the initialization module. The specific model structure is consistent with the structure used in the robustness test. All the data-driven baselines were trained on 2D synthetic

random graphs with $\sigma = 0.005$, $n_{in} = 50$, $n_{out} = 15$, and then directly applied to the real-world dataset. The optimizer settings in training are identical to the ones used in the robustness test experiment. In Table 1, “without-ensemble” denotes the model that the single QAP-solver is applied as a stand-alone traditional solver without any GNN feature extractor. It performs roughly 40 percent worse than the proposed ensemble model. Our ensemble model achieves the best performance, outperforming the previous best geometric matching method, DGMC [51]. Some examples of matching results on PASCAL-PF are shown in Figure 6.

Additionally, we conducted an experiment on the CMU-House dataset. For the traditional matching algorithms including PSM [4], GAGM [72], RRRw [54], SM [48], we build graphs by using these landmarks as nodes and adopting Delaunay tri-angulation to generate edges. For the deep learning matching approaches including DGFL [89], DGMC [51], PointNet [11], and our EQAN, we normalize the keypoint coordinates by subtracting the statistic mean and dividing by its statistic variance. We report the final average matching accuracy in Figure 3 under the frame gap setting of 10:10:100 frames. The results show that our method can keep a relatively good performance even when the number of inliers is small, and the frame gap is large.

6.3 Semantic feature matching

We evaluate the performance of semantic feature matching on PASCAL-VOC and Spair-71K datasets following the experimental protocol in [5,63,53,51,64].

6.3.1 PASCAL-VOC Keypoint

This dataset [49] contains 20 classes of instances and 7,020 annotated images for training and 1,682 for testing. Berkeley’s annotations provide labeled keypoint locations [49]. Following [5,65,63], we crop the bounding box around the object in the image and resized the cropped box to 256×256 . For baselines, we choose the following methods: PCA [63], GMN [5], CIE [76], CLDGM [62], LCSGM [74], DGMC [51], BBGM [53], NGM+ [64], QC-DGM [59], IA-DGM [37], GLMNet [9], SIGMA [43] and DLGM [77].

Training protocol By following [5,63,53,51,64], we build the graph by setting the keypoints as nodes and then using Delaunay triangulation to connect landmarks. The node features are generated from the conv4-2 and the conv5-1 layer of a pre-trained VGG-16 [39], which is fixed without further fine-tuning during training of GNN. Since the width and height of the feature map are smaller than the given image, we use the bilinear interpolation to approximately recover the node feature of the given landmark pixel in the image.

Table 1 Geometric graph matching accuracy on PASCAL-PF [55]. All data-driven matching approaches are trained on 2D synthetic random graphs and then directly applied to the dataset. The results of Pointnet [11] are reported in [89].

PASCAL-PF	aero	bike	bird	boat	bottle	bus	car	cat	chair	cow	table	dog	horse	mbike	person	plant	sheep	sofa	train	tv	mean
PointNet [11]	54.8	70.2	65.2	73.7	85.3	90.0	73.4	63.4	55.2	78.4	78.4	52.5	58.0	64.2	57.4	68.9	50.5	74.0	88.1	91.9	69.7
DGFL [89]	76.1	89.8	93.4	96.4	96.2	97.1	94.6	82.8	89.3	96.7	89.7	79.5	82.6	83.5	72.8	76.7	77.1	97.3	98.2	99.5	88.5
DGMC [51]	81.1	92.0	94.7	100.0	99.3	99.3	98.9	97.3	99.4	93.4	100.0	99.1	86.3	86.2	87.7	100.0	100.0	100.0	100.0	99.3	95.7
DPGM-Net [23]	79.3	92.5	97.7	96.4	94.6	96.4	96.3	95.7	98.3	95.0	76.3	90.7	85.1	84.7	88.8	65.2	100.0	100.0	100.0	67.2	90.6
without-ensemble	48.4	74.0	69.3	49.6	46.1	58.3	73.2	49.1	62.5	57.2	41.9	49.0	61.3	64.4	42.4	35.7	53.3	59.8	63.2	37.5	57.0
EQAN-R	85.7	90.6	86.9	98.3	90.1	88.0	98.6	94.5	91.7	91.8	99.3	87.7	79.1	79.8	83.1	88.1	95.8	93.5	85.1	93.2	90.3 ± 0.8
EQAN	87.2	91.5	94.6	98.4	99.4	99.1	98.9	99.5	99.6	95.7	100.0	99.6	90.5	89.4	88.7	100.0	100.0	99.2	99.6	99.6	96.2 ± 0.3
EQAN-U	87.7	91.1	90.8	98.8	99.8	98.9	99.1	97.0	100.0	96.0	100.0	100.0	90.8	89.6	89.1	100.0	100.0	99.6	99.1	100.0	96.4 ± 0.4

Table 2 Semantic feature matching accuracy on PASCAL VOC Keypoints. Results of GMN, PCA, and CIE are taken from [76]. The results of DGMC, NGM+, GLMNet are taken from [53]. The BBGM is implemented based on the official repository in [53]. The results of SIGMA are taken from Table 5 in the original article [43]. The per-class results of GAMnet [30] and ASAR-GM [60] are not available in their original papers.

method	aero	bike	bird	boat	bottle	bus	car	cat	chair	cow	table	dog	horse	mbike	person	plant	sheep	sofa	train	tv	mean
GMN [5]	31.9	47.2	51.9	40.8	68.7	72.2	53.6	52.8	34.6	48.6	72.3	47.7	54.8	51.0	38.6	75.1	49.5	45.0	83.0	86.3	55.3
PCA [63]	40.9	55.0	65.8	47.9	76.9	77.9	63.5	67.4	33.7	65.5	63.6	61.3	68.9	62.8	44.9	77.5	67.4	57.5	86.7	90.9	63.8
CLDGM [62]	51.0	64.9	68.4	60.5	80.2	74.7	71.0	73.5	42.2	68.5	48.9	69.3	67.6	64.8	48.6	84.2	69.8	62.0	79.3	89.3	66.9
LCSGM [74]	46.9	58.0	63.6	69.9	87.8	79.8	71.8	60.3	44.8	64.3	79.4	57.5	64.4	57.6	52.4	96.1	62.9	65.8	94.4	92.0	68.5
NGM+ [64]	50.8	64.5	59.5	57.6	79.4	76.9	74.4	69.9	41.5	62.3	68.5	62.2	62.4	64.7	47.8	78.7	66.0	63.3	81.4	89.6	66.1
GLMNet [9]	52.0	67.3	63.2	57.4	80.3	74.6	70.0	72.6	38.9	66.3	77.3	65.7	67.9	64.2	44.8	86.3	69.0	61.9	79.3	91.3	67.5
CIE [76]	51.2	69.2	70.1	55.0	82.8	72.8	69.0	74.2	39.6	68.8	71.8	70.0	71.8	66.8	44.8	85.2	69.9	65.4	85.2	92.4	68.9
IA-DGM [37]	53.9	67.7	68.8	60.2	80.3	75.1	76.9	72.0	40.2	65.6	79.6	65.4	66.2	67.4	46.3	87.4	65.4	58.5	89.4	90.7	68.8
QC-DGM [59]	49.6	64.6	67.1	62.4	82.1	79.9	74.8	73.5	43.0	68.4	66.5	67.2	71.4	70.1	48.6	92.4	69.2	70.9	90.9	92.0	70.3
DGMC [51]	50.4	67.6	70.7	70.5	87.2	85.2	82.5	74.3	46.2	69.4	69.9	73.9	73.8	65.4	51.6	98.0	73.2	69.6	94.3	89.6	73.2
BBGM [53]	61.5	75.0	78.1	80.0	87.4	93.0	89.1	80.2	58.1	77.6	76.5	79.3	78.6	78.8	66.7	97.4	76.4	77.5	97.7	94.4	80.0
SIGMA [43]	55.1	70.6	57.8	71.3	88.0	88.6	88.2	75.5	46.8	70.9	90.4	66.5	78.0	67.5	65.0	96.7	68.5	97.9	94.3	86.1	76.2
DLGM [77]	64.7	78.1	78.4	81.0	87.2	94.6	89.7	82.5	68.5	83.0	93.9	82.3	82.8	82.7	69.6	98.6	78.9	88.9	97.4	96.7	83.8
NGMv [64]	59.9	71.5	77.2	79.0	87.7	94.6	89.0	81.8	60.0	81.3	87.0	78.1	76.5	77.5	64.4	98.7	77.8	75.4	97.9	92.8	80.4
GAMnet [30]	-	-	-	-	-	-	-	-	-	-	-	-	-	-	-	-	-	-	-	-	80.7
ASAR-GM [60]	-	-	-	-	-	-	-	-	-	-	-	-	-	-	-	-	-	-	-	-	81.2
without-ensemble	49.7	64.8	57.3	57.1	78.4	81.2	66.3	69.6	45.2	63.4	64.2	63.5	67.9	62.0	46.8	85.5	70.7	58.1	88.9	89.9	66.5 ± 0.5
EQAN-R	59.9	59.3	71.2	63.5	85.9	77.6	71.1	83.2	46.1	58.5	99.2	72.9	80.8	65.4	58.6	79.5	74.2	51.0	90.4	80.9	71.5 ± 0.9
EQAN	66.4	74.4	82.6	71.0	88.7	87.7	86.4	80.4	53.4	66.6	100.0	80.3	78.0	76.7	64.6	96.5	83.7	62.2	100.0	95.5	79.8 ± 0.5
EQAN-U	68.5	76.9	81.9	71.2	89.1	91.3	82.0	82.9	52.0	70.9	100.0	80.9	78.8	79.3	66.7	95.7	87.4	65.7	100.0	96.8	80.9 ± 0.4

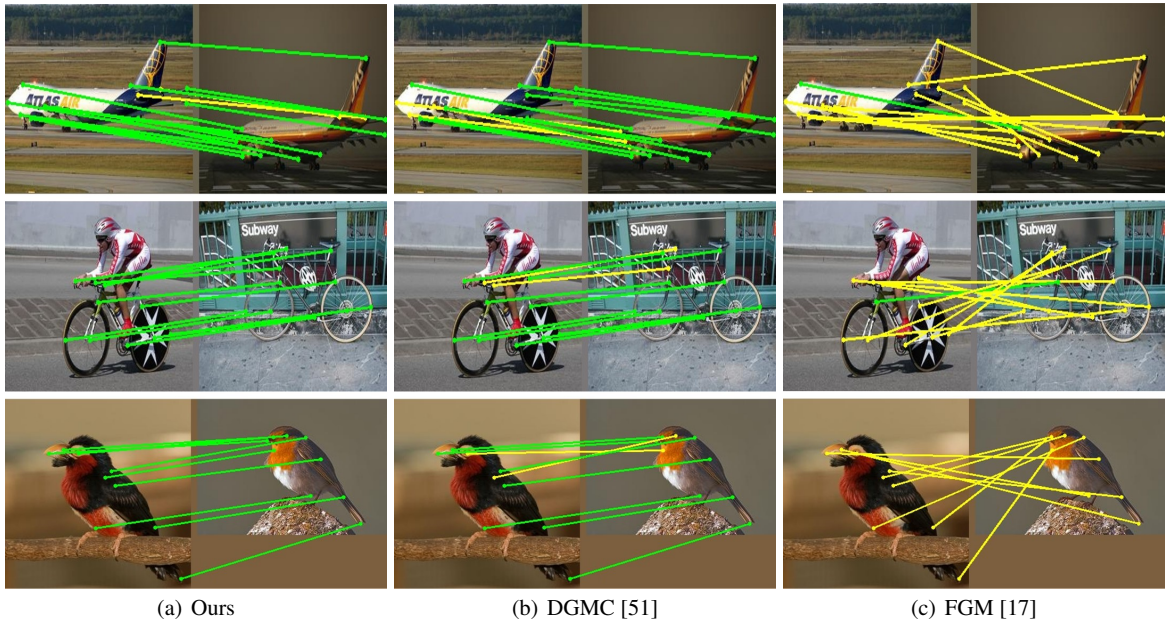
**Fig. 6** Typical matching results on PASCAL-PF. The green line indicates the matching is correct, and yellow means wrong. FGM [17] is one of the classical traditional graph matching methods. DGMC [51] and ours are both trained on synthetic graphs only.

Table 3 Semantic feature matching accuracy on Spair-71K. Results of DGMC, BBGM are taken from [53]. For SIGMA [43], the mean accuracy is 79.8 ± 0.2 , while the accuracy score per-class is not provided in [43].

method	aero	bike	bird	boat	bottle	bus	car	cat	chair	cow	dog	horse	mbike	person	plant	sheep	train	tv	mean
DGMC [51]	54.8	44.8	80.3	70.9	65.5	90.1	78.5	66.7	66.4	73.2	66.2	66.5	65.7	59.1	98.7	68.5	84.9	98.0	72.2
BBGM [53]	66.9	57.7	85.8	78.5	66.9	95.4	86.1	74.6	68.3	78.9	73.0	67.5	79.3	73.0	99.1	74.8	95.0	98.6	78.9
SIGMA [43]	-	-	-	-	-	-	-	-	-	-	-	-	-	-	-	-	-	-	79.8
DLGM [77]	70.4	66.8	86.7	81.7	69.2	96.4	85.8	79.5	78.4	84.0	79.4	69.4	84.5	76.6	99.1	75.9	96.4	98.5	82.0
without-ensemble	31.7	72.3	76.0	42.7	54.3	76.9	93.3	60.0	53.0	62.2	50.2	40.7	55.3	52.2	87.2	70.9	99.5	82.9	65.6 ± 0.1
EQAN-R	51.9	55.6	78.7	72.3	59.0	89.2	78.5	75.3	52.2	73.1	71.0	69.8	80.8	54.7	93.7	66.5	80.4	89.0	71.8 ± 0.8
EQAN	65.3	62.5	86.7	83.5	69.7	95.5	92.3	77.5	66.5	78.2	75.8	73.4	81.3	64.6	99.3	74.5	93.4	99.3	79.9 ± 0.5
EQAN-U	65.5	65.1	81.1	84.2	71.7	97.9	93.4	78.1	67.7	80.1	72.8	74.3	83.2	67.3	100.0	75.7	93.9	100.0	80.7 ± 0.3

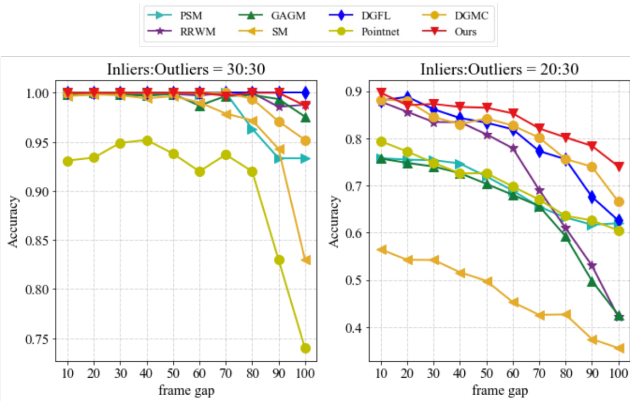


Fig. 7 Comparison of matching accuracy on the CMU-House dataset.

For our model, by following [53, 51, 77, 43], we adopt a SplineCNN network [50] as the GNN module in the initialization module to further refine the input semantic features from the VGG feature extractor. For constructing the ensemble assignment module, we set the number of proximal QAP-solver in each block to be $C = 32$ and set the block number $L = 5$. We also adopt the single proximal QAP-solver (DPGM) as the differentiable solver attached after the VGG-16 feature extractor as a baseline, see the item “without-ensemble”. It is also trained on the same dataset in an end-to-end fashion.

Table 2 gives the experimental results. Compared to the “without-ensemble”, our ensemble model with multiple proximal solvers (EQAN, EQAN-U) exhibits a considerable performance improvement of about 13%. The EQAN-U model outperforms DGMC [51], BBGM method [53], and SIGMA [43], by 7.7%, 0.9%, and 4.7% in matching accuracy respectively. Our EQAN achieves comparable performance with NGMv2 [64], GAMnet [30] and ASAR-GM [60]. Visual examples of the matching results on PASCAL-VOC are shown in Figure 8. Our work, mainly focused on the network architecture based on the connections between the ensemble of classical algorithms and the multi-channel graph neural networks, has the potential of further improvement by combining the idea of adversarial training used in ASAR-GM, but it requires more carefully-designed architecture with the corresponding training method. We leave this study for future work.

EQAN v.s. DLGM DLGM [77] proposed a complex but novel graph feature extractor, the core of which is to use a neural network to learn potential graph structure. It achieved an amazing accuracy of 83.8% on Pascal-VOC Keypoint and 82.0% on Spair-71K. However, the code of DLGM is still not open to the public. Considering the solver module in DLGM is just a simple traditional quadratic assignment algorithm, we believe that our deep ensemble model can also improve the performance of DLGM by taking it as a QAP solver in our framework.

6.3.2 Spair-71K

The SPair-71K [35] dataset contains 70,958 image pairs prepared from PASCAL-VOC 2012 and PASCAL 3D+. For our model, we adopt the same model architecture setting and training protocol as used on PASCAL-VOC Keypoints. DGMC [51], BBGM [53], DLGM [77] and SIGMA [43] are evaluated as comparison. The results in Table 3 show that our model consistently improves upon the baseline, the one without ensemble, and out-performances DGMC, BBGM and SIGMA, while is slightly lower than DLGM.

6.4 Few-shot 3D shape classification

We apply our model to the few-shot 3D shape classification task via point-cloud matching. The experiment was conducted on the ModelNet40 dataset [91], which consists of 12,311 meshed CAD models from 40 categories. In this dataset, the number of nodes in 3D shape objects is as large as thousands, causing computation challenges in graph matching. For few-shot classification, only 1 or 5 examples are used for each class for K-nearest neighbor classification. The selected classes are randomly sampled from 40 categories. We report the average accuracy of 20 independent runs.

We compare our method with representative previous methods: SPH [52] uses the Spherical Harmonics descriptor for shape classification; LFD [15] uses the Light Field descriptor for 3D shapes; FV [18] uses the Fisher vectors for the 3D object; MVCNN [21] and GIFT [71] adopt a CNN

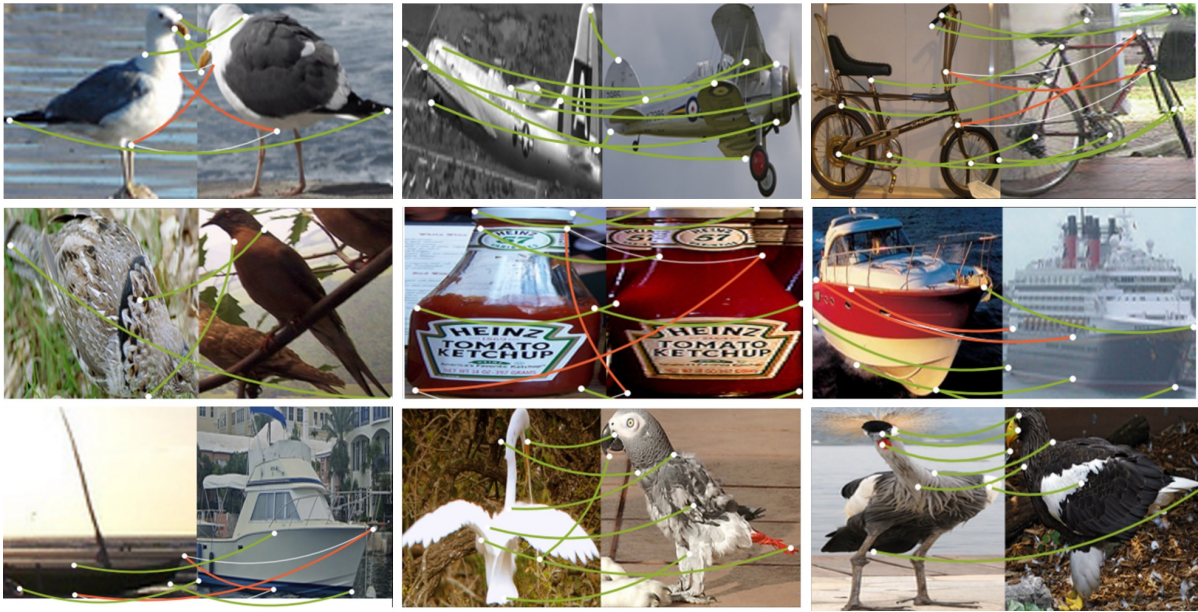


Fig. 8 Example semantic feature matching results of the proposed approach on PASCAL-VOC. Our method can handle pairs of images seen from very different viewpoints. The green line indicates the matching is correct, and red means wrong. The visualization code is based on the official code repository of [53].

Table 4 Accuracies of few-shot 3D shape classification on the ModelNet40 dataset. Results of SPH [52], LFD [15], FV [18], MVCNN [21], GIFT[71] and Meta-LSTM [32] are taken from [32]. MFSC’s results are taken from [61]. OOM indicates that the network caused a memory overflow.

Method	SPH [52]	LFD [15]	FV [18]	MVCNN [21]	GIFT[71]	Meta-LSTM [32]	MFSC [61]	EQAN	EQAN-U	EQAN-R
5-way-1-shot	28.86	41.08	43.13	44.90	43.25	45.46	68.10	OOM	OOM	66.24 ± 0.7
5-way-5-shot	49.79	51.04	55.96	58.94	53.40	62.57	73.20	OOM	OOM	84.71 ± 1.4

network to extract multi-view semantic features for a 3D object into multiple views; Meta-LSTM [32] uses a dual LSTM model to tackle the 3D few-shot problem; MFSC [61] is a model-agnostic approach for few-shot shape recognition.

Following the settings in [61, 32], we report the results of two scenarios: the 5-way-1-shot case and the 5-way-5-shot case, to classify 5 unseen classes. To test the models, we obtain the point cloud by uniformly sampling 1000 points from the surface of each CAD model. We normalize those coordinates by subtracting the statistic mean and dividing by its standard deviation. Then, we connect each point in the point cloud with their top-3 nearest neighbors.

We train our model using only 3D synthetic random graphs and only use the normalized coordinate information of keypoints as input node features. For constructing the ensemble model, the block number is set to be $L = 10$ and the solver number is $C = 6$ for each block. In addition, we use the random sampling mechanism introduced in Section 5.3 to reduce GPU memory usage. The classification is based on the similarity r between the query graph and the support graph. Let the matrix R be the reward matrix defined in (15), and Q be the output matching prediction defined in (16).

The similarity r is computed via $r = \text{tr}(QR)$, i.e., the inner product between Q and R .

The classification results are shown in Table 4. In the single-shot setting, our technique (EQAN-R) and MFSC [61] surpass all other methods by 20 percent. In the 5-shot circumstances, our technique (EQAN-R) outperformed the other methods by more than 10 percent, while the vanilla version (EQAN) and the model with affinity update (EQAN-U) cannot handle such large 3D point-cloud graphs.

6.5 Ablation study

We conduct a thorough ablation study to investigate which part makes the proposed ensemble-analogy GNN effective. Specifically, we first investigate how to fuse the ensemble of base solvers, where the naive average only yields matching accuracy of 37.0, and our EQAN with special designed connectivity reaches 99.1. Then, we study the effect of training the internal parameters in base solvers. Next, we show the difference among 4 types of base solvers. Additionally, we discuss the choice of input for making the final matching decision, and the effect of normalization layers. Finally, we

study hyper-parameter sensitivity, random sampling strategy and real running time.

The experiments are based on 2D synthetic graphs randomly generated with the number of inliers $n_{\text{in}} = 35$ and number of outliers $n_{\text{out}} = 15$, noise level $\sigma = 0.3$ and we use the k-neighbor nearest rule with $k = 3$ to generate the edges.

6.5.1 Our ensemble model v.s. naive ensemble average

In this experiment, we compare our ensemble model and the naive ensemble method. Our model inherits the idea of ensemble learning with a more involved structure, e.g. adding a 1×1 convolution to promote the information exchange among channels. The naive ensemble method, on the other hand, computes the matching estimation independently, and only performs the average over the very last output.

Specifically, we test a naive implementation of an ensemble model that the decision matrix generated by $\mathbf{Q} = \sum_i w_i \mathbf{z}_i$, where \mathbf{z}_i is the i th independent solver’s prediction, and w_i is a learnable weight. The experiment listed in Table 5(a) shows that the naive ensemble method does not gain any performance improvement compared to the single solver (denoted by w/o ensemble). This experiment indicates that the design of the ensemble architecture plays a crucial role.

6.5.2 Learn or fix the internal parameters \mathbf{w}

The parameters \mathbf{w} inside the proximal solver determine the optimization trajectory and convergence of the solver, as illustrated in Proposition 1 (in the Appendix). Manually determining the best parameters for all solvers in the network is nearly impossible. In our framework, the parameters are learned in an end-to-end way. In this experiment, we also implement a variant model in which the internal parameters are determined by random sampling between 0 and 1. As shown in Table 5(b), the learning model outperforms the random selection model demonstrating the necessity of learning the internal parameters.

6.5.3 Replace DPGM with other QAP-solvers

In this experiment, we test different QAP-solver in our ensemble model, namely the differentiable graduated assignment method (GAGM) [72], the differentiable (power-iteration based) spectrum method (SM) [5] and RRWM [54]. Specifically, we use them to construct an EQAN with $L = 5$ blocks, where each block contains 32 GAGM or SM solvers. For GAGM, by following the annealing strategy in [72], we set the internal parameter β for solver in the ℓ th block to be $\beta = 0.5 * 1.075^{\ell-1}$. These QAP-solvers can also be viewed as GNNs on the association graph. We put their pseudo-code in Appendix B for the readers’ convenience. The results

Table 5 Study the effect of architecture design on synthetic random graphs, where the underlined choices are adopted in our previous experiments.

Component	Choice	Accuracy
(a). Ensemble framework	w/o ensemble	37.4
	Averaging	37.0
	<u>EQAN</u>	99.1
(b). Internal parameters \mathbf{w}	Random	74.1
	<u>Learning</u>	99.1
(c). Ensemble with other solvers	DPGM-Single	37.1
	DPGM-Ensemble	99.1
	GAGM-Single	39.9
	GAGM-Ensemble	96.2
	SM-Single	38.6
	SM-Ensemble	94.7
	RRWM-Single	40.1
RRWM-Ensemble	99.4	
(d). Decision feature \mathbf{V}	Last one only	93.4
	<u>All blocks</u>	99.1
(e). Model width C	$C = 8$	79.1
	$C = 16$	89.2
	<u>$C = 32$</u>	99.1
	$C = 64$	99.3
(f). Model depth L	$L = 2$	79.2
	$L = 4$	98.1
	<u>$L = 5$</u>	99.1
	$L = 8$	99.2
	$L = 16$	98.9

shown in Table 5(c) demonstrate that the proposed ensemble model can significantly improve performance for all selected QAP solvers, which verifies the universality of our framework.

Interesting, EQAN with the base solver of RRWM have slightly better performance (99.4) than the one with DPGM (99.1). Compared with RRWM, DPGM and RRWM share similar unconstrained gradient update and the Sinkhorn operation. However, RRWM has additional normalization and momentum term, which may contribute to the additional improvement.

6.5.4 The decision feature: all blocks or last one only

In our model, the decision layer takes the feature tensor \mathbf{V} defined in (14) as the input feature. Originally, we concatenate output of all the EnsembleBlock. Here, we compare this decision feature with an alternative that only use the output of the last block $\mathbf{V} = \mathbf{V}^{(L)}$. Details are shown in Table 5(d). The experiment verifies that the model using all the features of all blocks is better than the one just using the last layer’s output.

6.5.5 Sinkhorn normalization layer

To study the effect of the Sinkhorn operation after each layer of GNN, we establish an experiment, in which we revised the GNN structure that only run a single Sinkhorn procedure before the decision layer. The accuracy decreases from the original 99.1% to 71.4% under the same setup as other ablation study. It indicates the Sinkhorn normalization plays an important role in the proposed GNN model. An intuitive explanation is the analogy of the Sinkhorn procedure as a (batch) normalization layer, which is a common module in convolutional neural networks, whereas the Sinkhorn procedure implements a more strictly, doubly stochastic normalization.

6.5.6 Hyper-parameters: width and depth

Next, we study how different width (C , the number of solvers in each block) and depth (L , the number of blocks in the model) affect the results. We test the width C from 8 to 64 while keeping the depth $L = 5$. Then, fixing the width $C = 32$, we change the depth L from 2 to 16. Experiments reveal that the width and depth have an optimal region, and within this region, the performance is stable. Details are shown in Table 5 component (e) and (f). In general, larger model results better performance, and the setting $C = 32$ and $L = 5$ is the best settings for balancing performance and model complexity.

6.5.7 The random sampling strategy

We conduct experiments to study the relation between the sampling size (number of sampled entries) and the matching accuracy. The random sampling strategy can reduce the GPU memory usage so that our model can scale up to thousand nodes. On the other hand, the random sampling trick can potentially affect the prediction accuracy. A moderate sampling size is important to balance the efficiency and the accuracy. We test different sampling size $N_s = \gamma n \sqrt{n}$ by changing the coefficient γ , where n is the number of nodes of the input graph. The experimental results are reported in Figure 9. It shows that when $\gamma > 1$, the performance will almost saturate. Larger γ does not lead to significant performance gains, but does increase the model complexity. Empirically, $\gamma = 1$ achieves the best trade-off between efficiency and accuracy.

In Table 6, we provide the comparison between our guided sampling scheme and the randomly sampling on PASCAL-PF. The results show that the proposed sampling scheme is better than the naive random sampling.

6.5.8 Running time for inference

Figure 10 shows the real running time of the vanilla EQAN, the EQAN with the affinity update scheme (EQAN-U), and

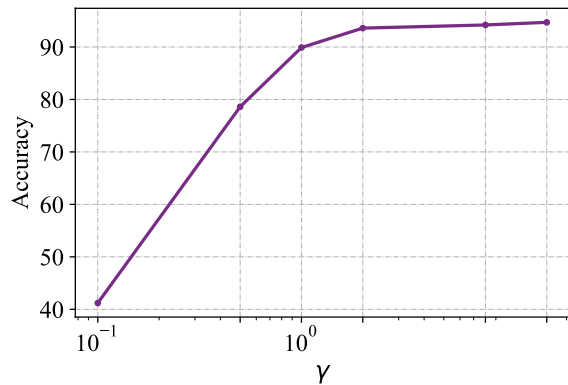


Fig. 9 Random sampling size v.s. matching accuracy. The graph matching accuracy under different sampling sizes γN_s with $N_s = n\sqrt{n} = 5400$.

Table 6 The EQAN with the proposed sampling scheme and the vanilla random sampling scheme.

Choice	Accuracy
Full messages (no sampling) [72]	96.2
Proposed sampling scheme	90.3
Vanilla random sampling scheme	81.9

the EQAN with the random sampling strategy (EQAN-R) as well as two peer methods, FGM [17] and BBGM [53], under different graph scales. Under the small graph setting ($N \leq 150$), the running time of three varieties of the proposed EQAN is less than one second, which is slower than the BBGM but significantly faster than the classic FGM algorithm. The vanilla EQAN model reaches the computational limit with more than 600 nodes. The affinity update scheme consumes more time, whereas the random sampling strategy allows the model to scale for the graphs up to 1000 nodes in a reasonable amount of time (about 15 seconds). We also note that when the graph size is small, the random sampling strategy does not significantly improve the inference speed of the model especially, as the sampling mask B breaks the vectorized parallel computation at the hardware implementation level.

7 Conclusion

This paper proposes a new graph neural network (GNN) that combines the advantage of both traditional graph matching algorithms and recently proposed graph neural network (GNN) based approaches. Specifically, we transform the previous traditional solvers as single-channel GNNs on the association graph and extend the single-channel architecture to the multi-channel network. The proposed model can be seen as an ensemble method that fuses multiple algorithms at every iteration in a parameterized way. In addition, we propose a random sampling strategy to reduce the computational

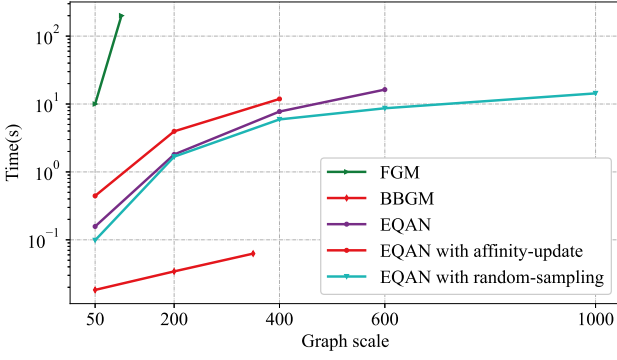


Fig. 10 Study on the random sampling strategy. The inference running time of the vanilla network (EQAN), the network with the affinity update scheme (EQAN-U), the network with the random sampling strategy (EQAN-R) as well as two peer methods FGM [17] and BBGM [53] under different graph scales.

complexity and GPU memory usage so as to improve the scalability of the model. Experimental results of geometric graph matching, semantic feature matching, and few-shot 3D shape classification demonstrate the superior performance, robustness, and scalability of our approach.

Acknowledgements

This work has been supported by the Major Project for New Generation of AI under Grant No. 2018AAA0100400, the National Natural Science Foundation of China (NSFC) grants U20A20223, 61836014, 61721004, the Youth Innovation Promotion Association of CAS under Grant 2019141, and the Pioneer Hundred Talents Program of CAS under Grant Y9S9MS08 and Y9S9MS08.

Appendix

A Convergence analysis and derivation of the differentiable proximal graph matching algorithm

In this section, we show that under a mild assumption, the proximal graph matching algorithm converges to a stationary point within a reasonable number of iterations. The main technique in this analysis follows [41], which studied a general variational inference problem using the proximal-gradient method.

Before presenting the main proposition, we first show a technical lemma.

Lemma 1 *There exist a constant $\alpha > 0$ such that for all $\mathbf{z}_{t+1}, \mathbf{z}_t$ generated during the forward pass of the solver, we have*

$$(\mathbf{z}_{t+1} - \mathbf{z}_t)^\top \nabla_{\mathbf{z}_{t+1}} D(\mathbf{z}_{t+1}, \mathbf{z}_t) \geq \alpha \|\mathbf{z}_{t+1} - \mathbf{z}_t\|^2,$$

where D is the KL-divergence.

We note that the largest valid α satisfying Lemma 1 is $1/2$. One can find the proofs of both this lemma and the proposition shown below in the appendix. Next, we show the main result of our convergence analysis.

Proposition 1 *Let L be the Lipschitz constant of the gradient function $\nabla g(\mathbf{z})$, where $g(x)$ is defined in (3), and let α be the constant used in Lemma 1. If we choose a constant step-size $\beta < 2\alpha/L$ for all $t \in \{0, 1, \dots, T\}$, then*

$$\mathbb{E}_{t \sim \text{uniform}\{0,1,\dots,T\}} \|\mathbf{z}_{t+1} - \mathbf{z}_t\|^2 \leq \frac{C_0}{T(\alpha - L\beta/2)},$$

where $C_0 = |\mathcal{L}^* - \mathcal{L}(\mathbf{z}_0)|$ is the objective gap of (2) between the initial guess $\mathcal{L}(\mathbf{z}_0)$ and the optimal one \mathcal{L}^* .

Proposition 1 guarantees that the iterative process converges to a stationary point within a reasonable number of iterations. In particular, the average difference $\|\mathbf{z}_{t+1} - \mathbf{z}_t\|^2$ of the iterand converges with a rate $1/T$.

A.1 Proof of the Lemma 1

Because the proximal function $D(\mathbf{z}, \mathbf{z}_t)$ is convex, the following inequality always hold:

$$D(\mathbf{z}_t, \mathbf{z}_t) \geq D(\mathbf{z}_{t+1}, \mathbf{z}_t) + [\nabla_{\mathbf{z}=\mathbf{z}_{t+1}} D(\mathbf{z}, \mathbf{z}_t)]^\top (\mathbf{z}_t - \mathbf{z}_{t+1}).$$

By using $D(\mathbf{z}_t, \mathbf{z}_t) = 0$, we obtain:

$$D(\mathbf{z}_{t+1}, \mathbf{z}_t) \leq (\mathbf{z}_{t+1} - \mathbf{z}_t)^\top [\nabla_{\mathbf{z}=\mathbf{z}_{t+1}} D(\mathbf{z}, \mathbf{z}_t)].$$

Let $l(\mathbf{z}) = \mathbf{z}^\top \log \mathbf{z}$. We decompose $D(\mathbf{z}_t, \mathbf{z}_t)$ as the following form of bregman divergence:

$$D(\mathbf{z}_{t+1}, \mathbf{z}_t) = l(\mathbf{z}_{t+1}) - l(\mathbf{z}_t) - \nabla l(\mathbf{z}_t)^\top (\mathbf{z}_{t+1} - \mathbf{z}_t).$$

Moreover, due to the strong convexity of $l(\mathbf{z})$,

$$l(\mathbf{z}_{t+1}) - l(\mathbf{z}_t) - \nabla l(\mathbf{z}_t)^\top (\mathbf{z}_{t+1} - \mathbf{z}_t) \geq \frac{1}{2} \|\mathbf{z}_{t+1} - \mathbf{z}_t\|^2,$$

then we get:

$$\frac{1}{2} \|\mathbf{z}_{t+1} - \mathbf{z}_t\|^2 \leq D(\mathbf{z}_{t+1}, \mathbf{z}_t) \leq (\mathbf{z}_{t+1} - \mathbf{z}_t)^\top \nabla D(\mathbf{z}_{t+1}, \mathbf{z}_t),$$

which proves lemma 1 and suggests that the largest valid α is $\frac{1}{2}$.

A.2 Proof of the Proposition 1

Before the proof of the proposition 1, we first present a technical lemma.

Lemma 2 *For any real-valued vector \mathbf{g} which has the same dimension of \mathbf{z} and $\beta > 0$, considering the convex problem*

$$\mathbf{z}_{t+1} = \underset{\mathbf{z}=I}{\text{argmin}} : \{\mathbf{z}^\top \mathbf{g} - h(\mathbf{z}) + \frac{1}{\beta} D(\mathbf{z}, \mathbf{z}_t)\}, \quad (21)$$

where $h(\mathbf{z}) = -\lambda \mathbf{z}^\top \log(\mathbf{z})$ and D is the KL-divergence, the following inequality always holds:

$$\mathbf{g}^\top (\mathbf{z}_t - \mathbf{z}_{t+1}) \geq \frac{\alpha}{\beta} \|\mathbf{z}_t - \mathbf{z}_{t+1}\|^2 - [h(\mathbf{z}_{t+1}) - h(\mathbf{z}_t)].$$

Because of the convexity of the objective in the sub-problem, it is easy to derive that, if \mathbf{z}^* is the optimal, the following hold:

$$(\mathbf{z}^* - \mathbf{z}_t)^\top (\mathbf{g} - \nabla h(\mathbf{z}^*) + \frac{1}{\beta} \nabla D(\mathbf{z}^*, \mathbf{z}_t)) \leq 0.$$

Let $\mathbf{z}^* = \mathbf{z}_{t+1}$, by using lemma 1 we obtain that

$$\mathbf{g}^\top (\mathbf{z}_t - \mathbf{z}_{t+1}) - (\mathbf{z}_t - \mathbf{z}_{t+1})^\top \nabla h(\mathbf{z}_{t+1}) - \frac{\alpha}{\beta} \|\mathbf{z}_{t+1} - \mathbf{z}_t\|^2 \geq 0. \quad (22)$$

Because the entropic function $h(\mathbf{z})$ is concave, hence

$$(\mathbf{z}_t - \mathbf{z}_{t+1})^\top \nabla h(\mathbf{z}_{t+1}) \geq h(\mathbf{z}_t) - h(\mathbf{z}_{t+1}). \quad (23)$$

We can derive the following inequality from (22) and (23):

$$\mathbf{g}^\top (\mathbf{z}_t - \mathbf{z}_{t+1}) - [h(\mathbf{z}_t) - h(\mathbf{z}_{t+1})] - \frac{\alpha}{\beta} \|\mathbf{z}_{t+1} - \mathbf{z}_t\|^2 \geq 0,$$

which proves lemma 2.

Now, we start to prove Proposition 1.

Proof : Because $g(\mathbf{z})$ is L -Lipschitz gradient continuous, we get

$$g(\mathbf{z}_{t+1}) \leq g(\mathbf{z}_t) + \nabla g(\mathbf{z}_t)^\top (\mathbf{z}_{t+1} - \mathbf{z}_t) + \frac{L}{2} \|\mathbf{z}_{t+1} - \mathbf{z}_t\|^2. \quad (24)$$

Let $\mathbf{g} = \nabla g(\mathbf{z}_t)$. By using lemma 2, we bound the right side of (24) by

$$g(\mathbf{z}_{t+1}) \leq g(\mathbf{z}_t) - \frac{\alpha}{\beta} \|\mathbf{z}_t - \mathbf{z}_{t+1}\|^2 - [h(\mathbf{z}_t) - h(\mathbf{z}_{t+1})] + \frac{L}{2} \|\mathbf{z}_{t+1} - \mathbf{z}_t\|^2. \quad (25)$$

Rearranging the terms in (25) and noting that $g(\mathbf{z}) - h(\mathbf{z}) = L(\mathbf{z})$, we get

$$\left(\frac{\alpha}{\beta} - \frac{L}{2}\right) \|\mathbf{z}_{t+1} - \mathbf{z}_t\|^2 \leq \mathcal{L}(\mathbf{z}_t) - \mathcal{L}(\mathbf{z}_{t+1}).$$

Next, we choose a constant step-size $\beta < 2\alpha/L$ for all $t \in \{0, 1, \dots, T\}$. By summing both side from index of 0 to T , we have

$$\begin{aligned} \frac{1}{T} \sum_{t=0}^T \left(\frac{\alpha}{\beta} - \frac{L}{2}\right) \|\mathbf{z}_{t+1} - \mathbf{z}_t\|^2 &\leq \frac{\mathcal{L}(\mathbf{z}_0) - \mathcal{L}(\mathbf{z}_T)}{T} \\ &\leq \frac{\mathcal{L}(\mathbf{z}_0) - \mathcal{L}^*}{T}, \end{aligned}$$

and finally reach

$$\mathbb{E}_{t \sim \text{uniform}\{0, 1, \dots, T\}} \|\mathbf{z}_{t+1} - \mathbf{z}_t\|^2 \leq \frac{\mathcal{L}(\mathbf{z}_0) - \mathcal{L}^*}{T(\alpha - L\beta/2)}.$$

A.3 Derivation of DPGM Algorithm

Our proximal graph matching solves a sequence of convex optimization problems

$$\begin{aligned} \mathbf{z}_{t+1} = \underset{\mathbf{z} \in \mathbb{R}_+^{n^2 \times 1}}{\operatorname{argmin}} \quad & -\mathbf{z}^\top (\mathbf{u} + \mathbf{P}\mathbf{z}_t) + \frac{1+\beta_t}{\beta_t} \mathbf{z}^\top \log(\mathbf{z}) - \frac{1}{\beta_t} \mathbf{z}^\top \log(\mathbf{z}_t) \\ \text{s.t.} \quad & \mathbf{C}\mathbf{z} = \mathbf{1}. \end{aligned}$$

where the binary matrix $\mathbf{C} \in \{0, 1\}^{n^2 \times n^2}$ encodes n^2 linear constraints ensuring that $\sum_{i \in V_1} x_{ij'} = 1$ and $\sum_{j \in V_2} x_{ij'} = 1$ for all $i' \in V_1$ and $j' \in V_2$. We set

$$E_t(\mathbf{z}) = -\mathbf{z}^\top (\mathbf{u} + \mathbf{P}\mathbf{z}_t) + \frac{1+\beta_t}{\beta_t} \mathbf{z}^\top \log(\mathbf{z}) - \frac{1}{\beta_t} \mathbf{z}^\top \log(\mathbf{z}_t)$$

The matching objective with Lagrange multipliers for each sub-problem is

$$\mathcal{L}(\mathbf{z}, \boldsymbol{\mu}, \boldsymbol{\nu}) = E_t(\mathbf{z}) + \boldsymbol{\mu}^\top (\mathbf{Z}\mathbf{1} - \mathbf{1}) + \boldsymbol{\nu}^\top (\mathbf{Z}^\top \mathbf{1} - \mathbf{1}),$$

where $\boldsymbol{\mu}$ and $\boldsymbol{\nu}$ are Lagrange multipliers, and \mathbf{Z} is the matrix form of vector \mathbf{z} , which should be a doubly stochastic matrix. Setting derivatives $\frac{\partial \mathcal{L}}{\partial \mathbf{z}}, \frac{\partial \mathcal{L}}{\partial \boldsymbol{\mu}}, \frac{\partial \mathcal{L}}{\partial \boldsymbol{\nu}}$ be 0, we get

$$[\mathbf{z}]_{ij} = \exp \left[\frac{\beta_t}{1+\beta_t} [\mathbf{u} + \mathbf{P}\mathbf{z}_t]_{ij} + \frac{1}{1+\beta_t} \log([\mathbf{z}_t]_{ij}) + 1 + \frac{\beta_t}{1+\beta_t} ([\boldsymbol{\mu}]_j + [\boldsymbol{\nu}]_i) \right]$$

$$\sum_{i'=1}^n [\mathbf{z}]_{i'} = 1, \quad \sum_{j'=1}^n [\mathbf{z}]_{ij'} = 1,$$

for all $i, j \in 1, 2, \dots, n$. The solution of the above equations yields the following update rule [81,87]

$$\tilde{\mathbf{z}}_{t+1} = \exp \left[\frac{\beta_t}{1+\beta_t} (\mathbf{u} + \mathbf{P}\mathbf{z}_t) + \frac{1}{1+\beta_t} \log(\mathbf{z}_t) \right] \quad (26)$$

$$\mathbf{z}_{t+1} = \operatorname{Sinkhorn}(\tilde{\mathbf{z}}_{t+1}), \quad (27)$$

where $\operatorname{Sinkhorn}(\mathbf{z})$ is the Sinkhorn-Knopp transform [69] that maps a nonnegative matrix of size $n \times n$ to a doubly stochastic matrix. Here, the input and output variables are n^2 vectors. When using the Sinkhorn-Knopp transform, we reshape the input (output) as an $n \times n$ matrix (n^2 -dimensional vector) respectively.

Given a nonnegative matrix $\mathbf{F} \in \mathbb{R}_+^{n \times n}$, Sinkhorn algorithm works iteratively. In each iteration, it normalizes all its rows via the following equation:

$$\mathbf{F}'_{ij} = \mathbf{F}'_{ij} / \left(\sum_{k=1}^n \mathbf{F}_{ik} \right),$$

then it takes the column normalization by the following rule:

$$\mathbf{F}_{ij} = \mathbf{F}_{ij} / \left(\sum_{k=1}^n \mathbf{F}'_{kj} \right),$$

After processing iteratively until convergence, the original matrix \mathbf{F} would be transformed into a doubly stochastic matrix. Equation (26) and (27) lead to the proximal iteration (4) and (5).

B Additional pseudo-code of QAP solvers

We presented the pseudocodes of the related classical matching algorithms, GAGM and spectral method (SM) for readers' reference. Details are shown in Algorithm 3 and 4 respectively.

Algorithm 3 : Graduated assignment (GAGM)

Input: Affinity matrix \mathbf{M} , maximum iteration K , the annealing factor $\{\beta_1, \dots, \beta_K\}$.

Initialization: as the uniform starting solution \mathbf{x}_0 .

for $k = 1$ **to** K **do**

$$\hat{\mathbf{x}}_k = \underbrace{\mathbf{M}\mathbf{x}_{k-1}}_{\text{Message passing}}$$

$$\mathbf{x}_k = \underbrace{\operatorname{Sinkhorn}(\exp(\beta_k \hat{\mathbf{x}}_k))}_{\text{Normalization}}$$

end for

Output: \mathbf{x}_K

Algorithm 4 : Power-method based spectral method (SM)**Input:** Affinity matrix M , and maximum iteration K .**Initialization:** the uniform solution x_0 .**for** $k = 1$ **to** K **do**

$$\hat{x}_k = \underbrace{Mx_{k-1}}_{\text{Message passing}}$$

$$x_k = \underbrace{\hat{x}_k / \|\hat{x}_k\|}_{\text{Normalization}}$$

end for**Output:** x_K **References**

1. Weiyue Wang, Weiyao Lin, Yuanzhe Chen, Jianxin Wu, Jingdong Wang, Bin Sheng: Finding coherent motions and semantic regions in crowd scenes: a diffusion and clustering approach. In: European Conference on Computer Vision (2014)
2. Adam Paszke, Sam Gross, Soumith Chintala, G Chanan, E Yang, Zachary Devito, Zeming Lin, Alban Desmaison, L Antiga, A Lerer, et.al.: Automatic differentiation in pytorch. In: Advances in neural information processing systems Workshop (2017)
3. Alexander Berg, Tamara Berg, Jitendra Malik: Shape matching and object recognition using low distortion correspondences. In: Proceedings of the IEEE Conference on Computer Vision and Pattern Recognition (2005)
4. Amir Egozi, Yosi Keller, Hugo Guterman: A probabilistic approach to spectral graph matching. *IEEE Transactions on Pattern Analysis and Machine Intelligence* **35**(1), 18–27 (2013)
5. Andrei Zanfir, Cristian Sminchisescu: Deep learning of graph matching. In: Proceedings of the IEEE Conference on Computer Vision and Pattern Recognition (2018)
6. Bangpeng Yao, Feifei Li: Action recognition with exemplar based 2.5 d graph matching. In: European Conference on Computer Vision (2012)
7. Bengio, Y., Léonard, N., Courville, A.C.: Estimating or propagating gradients through stochastic neurons for conditional computation. *CoRR* **abs/1308.3432** (2013)
8. Benoit Huet, Edwin R. Hancock: Shape recognition from large image libraries by inexact graph matching. *Pattern Recognition Letters* **20**(11), 1259 – 1269 (1999)
9. Bo Jiang, Pengfei Sun, Jin Tang, Bin Luo: Glnet: Graph learning-matching networks for feature matching. In: arXiv preprint arXiv:1911.07681 (2019)
10. Chang Liu, Runzhong Wang, Zetian Jiang, Junchi Yan: Deep reinforcement learning of graph matching. In: arxiv preprint abs/2012.08950 (2020)
11. Charles Ruizhongtai Qi, Hao Su, Kaichun Mo, Leonidas Guibas: Pointnet: Deep learning on point sets for 3d classification and segmentation. In: Proceedings of the IEEE Conference on Computer Vision and Pattern Recognition (2017)
12. Chung-Shou Liao, Kanghao Lu, Michael Baym, Rohit Singh, Bonnie Berger: Isorankn: spectral methods for global alignment of multiple protein networks. In: *Bioinformatics* (2009)
13. Cristina Gomila, Fernand Meyer: Graph-based object tracking. In: Proceedings International Conference on Image Processing (2003)
14. Diederik P. Kingma, Jimmy Ba: Adam: A method for stochastic optimization. In: International Conference for Learning Representations (2015)
15. Ding-Yun Chen, Xiao-Pei Tian, Yu-Te Shen, Ming Ouhyoung: On visual similarity based 3d model retrieval. *Computer Graphics Forum* **22**(3), 223–232 (2003)
16. Dinggang Shen, Christos Davatzikos: Hierarchical attribute matching mechanism for elastic registration. *IEEE Transactions on Medical Imaging* **21**(11), 1421–1439 (2002)
17. Feng Zhou, De la Torre: Factorized graph matching. In: Proceedings of the IEEE Conference on Computer Vision and Pattern Recognition (2012)
18. Florent Perronnin, Christopher Dance: Fisher kernels on visual vocabularies for image categorization. In: Proceedings of the IEEE Conference on Computer Vision and Pattern Recognition (2007)
19. Fu-Dong Wang, Nan Xue, Yipeng Zhang, Gui-Song Xia, Marcello Pelillo: A functional representation for graph matching. *IEEE Transactions on Pattern Analysis and Machine Intelligence* **42**(11), 2737–2754 (2020)
20. Hailin Yu, Weicai Ye, Youji Feng, Hujun Bao, Guofeng Zhang: Learning bipartite graph matching for robust visual localization. In: IEEE International Symposium on Mixed and Augmented Reality (2020)
21. Hang Su, Subhransu Maji, Evangelos Kalogerakis, Erik Learned-Miller: Multi-view convolutional neural networks for 3d shape recognition. In: IEEE International Conference on Computer Vision (2015)
22. Hao Li, Asim Kadav, Igor Durdanovic, Hanan Samet, Hans Peter Graf: Pruning filters for efficient convnets. In: International Conference on Learning Representations (2017)
23. Hao-Ru Tan, Chuang Wang, Si-Tong Wu, Tie-Qiang Wang, Xu-Yao Zhang, Cheng-Lin Liu: Proxy graph matching with proximal matching networks. In: Proceedings of the AAAI Conference on Artificial Intelligence (2021)
24. Harold W Kuhn: The hungarian method for the assignment problem. *Naval research logistics quarterly* (1955)
25. Hongfang Wang, Hancock Edwin: A kernel view of spectral point pattern matching. In: Structural, Syntactic, and Statistical Pattern Recognition, pp. 361–369 (2004)
26. HongXia Wang, Xiang Chen, Chun Liu: Pose-guided part matching network via shrinking and reweighting for occluded person re-identification. *Image and Vision Computing* **111**, 104186 (2021)
27. Hwann-Tzong Chen, Horng-Horng Lin, Tyng-Luh Liu: Multi-object tracking using dynamical graph matching. In: Proceedings of the IEEE Conference on Computer Vision and Pattern Recognition (2001)
28. Jeremy Chopin, Jean-Baptiste Fasquel, Harold Mouchère, Rozenn Dahyot, Isabelle Bloch: Semantic image segmentation based on spatial relationships and inexact graph matching. In: Tenth International Conference on Image Processing Theory, Tools and Applications (IPTA) (2020)
29. Jianfeng He, Tianzhu Zhang, Yuhui Zheng, Mingliang Xu, Yongdong Zhang, Feng Wu: Consistency graph modeling for semantic correspondence. *IEEE Transactions on Image Processing* **30**, 4932–4946 (2021)
30. Jiang, B., Sun, P., Zhang, Z., Tang, J., Luo, B.: Gamnet: Robust feature matching via graph adversarial-matching network. In: MM '21: ACM Multimedia Conference 2021, pp. 5419–5426. ACM (2021)
31. Jiawei He, Zehao Huang, Naiyan Wang, Zhaoxiang Zhang: Learnable graph matching: Incorporating graph partitioning with deep feature learning for multiple object tracking. In: Proceedings of the IEEE Conference on Computer Vision and Pattern Recognition (2021)
32. Jie Nie, Ning Xu, Ming Zhou, Ge Yan, Zhiqiang Wei: 3d model classification based on few-shot learning. *Neurocomputing* **398**, 539–546 (2020)
33. Jiewen Zhao, Ruize Han, Yiyang Gan, Liang Wan, Wei Feng, Song Wang: Human identification and interaction detection in cross-view multi-person videos with wearable cameras. In: Proceedings of the ACM International Conference on Multimedia (2020)
34. Joseph Menke, Allen Yang: Graduated assignment graph matching for realtime matching of image wireframes. In: 2020 IEEE/RSJ International Conference on Intelligent Robots and Systems (2020)
35. Juhong Min, Jongmin Lee, Jean Ponce, Minsu Cho: Spair-71k: A large-scale benchmark for semantic correspondence. arXiv preprint arXiv:1908.10543 (2019)

36. Junchi Yan, Xucheng Yin, Weiyao Lin, Cheng Deng, Hongyuan Zha, Xiaokang Yang: A short survey of recent advances in graph matching. In: The Annual ACM International Conference on Multimedia Retrieval (2016)
37. Kaixuan Zhao, Shikui Tu, Lei Xu: Ia-gm: A deep bidirectional learning method for graph matching. In: Proceedings of the AAAI Conference on Artificial Intelligence (2021)
38. Kaleem Siddiqi, Ali Shokoufandeh, Sven Dickenson, Steven Zucker: Shock graphs and shape matching. In: IEEE International Conference on Computer Vision (1998)
39. Karen Simonyan, Andrew Zisserman: Very deep convolutional networks for large-scale image recognition. In: International Conference on Learning Representations (2015)
40. Kexue Fu, Shaolei Liu, Xiaoyuan Luo, Manning Wang: Robust point cloud registration framework based on deep graph matching. In: Proceedings of the IEEE Conference on Computer Vision and Pattern Recognition (2021)
41. Khan Mohammad Emtiyaz, Baque Pierre, Fleuret François, Fua Pascal: Kullback-leibler proximal variational inference. In: Advances in Neural Information Processing Systems 28 (2015)
42. Leordeanu Marius, Hebert Martial, Rahul Sukthankar: An integer projected fixed point method for graph matching and map inference. In: Advances in Neural Information Processing Systems (2009)
43. Linfeng Liu, Michael Hughe, Soha Hassoun, Liping Liu: Stochastic iterative graph matching. In: Proceedings of the 38th International Conference on Machine Learning (2021)
44. Liu, J., Chen, Y., Ye, X., Qi, X.: Prior-free category-level pose estimation with implicit space transformation. arXiv preprint arXiv:2303.13479 (2023)
45. Marcelo Fiori, Pablo Sprechmann, Joshua Vogelstein, Pablo Muse, Guillermo Sapiro: Robust multimodal graph matching: Sparse coding meets graph matching. In: Advances in neural information processing systems (2013)
46. Marco Carcassoni, Edwin R. Hancock: Spectral correspondence for point pattern matching. *Pattern Recognition* **36**(1), 193 – 204 (2003)
47. Mario Vento: A long trip in the charming world of graphs for pattern recognition. *Pattern Recognition* **48**(2), 291–301 (2015)
48. Marius Leordeanu, Martial Hebert: A spectral technique for correspondence problems using pairwise constraints. In: IEEE International Conference on Computer Vision (2005)
49. Mark Everingham, Luc Van Gool, Chris Williams, John WinnAndrew, Andrew Zisserman: The pascal visual object classes (voc) challenge. *International Journal of Computer Vision* **88**(2), 303–338 (2010)
50. Matthias Fey, Jan Eric Lenssen, Frank Weichert, Heinrich Müller: Splinecnn: Fast geometric deep learning with continuous b-spline kernels. In: Proceedings of the IEEE Conference on Computer Vision and Pattern Recognition (2018)
51. Matthias Fey, Jan Lenssen, Christopher Morris, Jonathan Masci, NilsM Kriege: Deep graph matching consensus. In: International Conference on Learning Representations (2020)
52. Michael Kazhdan, Thomas Funkhouser, Szymon Rusinkiewicz: Rotation invariant spherical harmonic representation of 3D shape descriptors. In: Symposium on Geometry Processing (2003)
53. Michal Rolínek, Paul Swoboda, Dominik Zietlow, Anselm Paulus, Vít Musil, Georg Martius: Deep graph matching via blackbox differentiation of combinatorial solvers. In: European Conference on Computer Vision (2020)
54. Minsu Cho, Jungmin Lee, Kyoung Mu Lee: Reweighted random walks for graph matching. In: European Conference on Computer Vision (2010)
55. Minsu Cho, Karteek Alahari, Jean Ponce: Learning graphs to match. In: Proceedings of the IEEE Conference on Computer Vision and Pattern Recognition (2013)
56. Neal Parikh, Stephen Boyd: Proximal algorithms. *Found. Trends Optim.* **1**(3), 127–239 (2014)
57. Pasquale Foggia, Gennaro Percannella, Mario Vento: Graph matching and learning in pattern recognition in the last 10 years. *International Journal of Pattern Recognition and Artificial Intelligence* **33**(1) (2014)
58. Penghang Yin, Jiancheng Lyu, Shuai Zhang, Stanley Osher, Yingyong Qi, Jack Xin: Understanding straight-through estimator in training activation quantized neural nets. In: International Conference on Learning Representations (2019)
59. Quankai Gao, Fudong Wang, Nan Xue, Jin-Gang Yu, Gui-Song Xia: Deep graph matching under quadratic constraint. In: Proceedings of the IEEE Conference on Computer Vision and Pattern Recognition (2021)
60. Ren, Q., Bao, Q., Wang, R., Yan, J.: Appearance and structure aware robust deep visual graph matching: Attack, defense and beyond. In: 2022 IEEE/CVF Conference on Computer Vision and Pattern Recognition (CVPR), pp. 15242–15251 (2022)
61. Rishi Puri, Avidesh Zakhori, Raul Puri: Few shot learning for point cloud data using model agnostic meta learning. In: International Conference on Image Processing (2020)
62. Run-Zhong Wang, Jun-Chi Yan, Xiao-Kang Yang: Combinatorial learning of robust deep graph matching: an embedding based approach. *IEEE Transactions on Pattern Analysis and Machine Intelligence* pp. 1–1 (2020)
63. Runzhong Wang, Junchi Yan, Xiaokang Yang: Learning combinatorial embedding networks for deep graph matching. In: IEEE International Conference on Computer Vision (2019)
64. Runzhong Wang, Junchi Yan, Xiaokang Yang: Neural graph matching network: Learning lawler’s quadratic assignment problem with extension to hypergraph and multiple-graph matching. In: arXiv preprint arXiv/1911.11308 (2019)
65. Runzhong Wang, Junchi Yan, Xiaokang Yang: Combinatorial learning of robust deep graph matching: an embedding based approach. *IEEE Transactions on Pattern Analysis and Machine Intelligence* pp. 1–1 (2020)
66. Runzhong Wang, Junchi Yan, Xiaokang Yang: Graduated assignment for joint multi-graph matching and clustering with application to unsupervised graph matching network learning. In: Advances in Neural Information Processing Systems (2020)
67. Scarselli Franco, Gori Marco, Tsoi Chung Ah, Hagenbuchner Markus, Monfardini Gabriele: The graph neural network model. *IEEE Trans. Neural Networks* **20**(1), 61–80 (2009)
68. Shaofeng Zeng, Zhiyong Liu, Xu Yang: Supervised learning for parameterized koopmans–beckmann’s graph matching. *Pattern Recognition Letters* **143**, 8–13 (2021)
69. Sinkhorn Richard, Knopp Paul: Concerning nonnegative matrices and doubly stochastic matrices. *Pacific J. Math.* **21**(2), 343–348 (1967)
70. Solomon Justin, Peyre Gabriel, Kim Vladimir, Sra Suvrit: Entropic metric alignment for correspondence problems. *ACM Transactions on Graphics* **35**(4) (2016)
71. Song Bai, Xiang Bai, Zhichao Zhou, Zhaoxiang Zhang, Jan Latecki Longin: Gift: A real-time and scalable 3d shape search engine. In: Proceedings of the IEEE Conference on Computer Vision and Pattern Recognition (2016)
72. Steven N Gold, Rangarajan Anand: A graduated assignment algorithm for graph matching. *IEEE Transactions on Pattern Analysis and Machine Intelligence* **18**(4), 377–388 (1996)
73. Tao Wang, Haibin Ling: Gracker: A graph-based planar object tracker. *IEEE Transactions on Pattern Analysis and Machine Intelligence* **40**(6), 1494–1501 (2018)
74. Tao Wang, He Liu, Yidong Li, Yi Jin, Xiaohui Hou, Haibin Ling: Learning combinatorial solver for graph matching. In: Proceedings of the IEEE Conference on Computer Vision and Pattern Recognition (2020)
75. Terry Caelli, Tiberio Caetano: Graphical models for graph matching: Approximate models and optimal algorithms. *Pattern Recognition Letters* **26**(3), 339 – 346 (2005)

76. Tianshu Yu, Runzhong Wang, Junchi Yan, Baoxin Li: Learning deep graph matching with channel-independent embedding and hungarian attention. In: International Conference on Learning Representations (2020)
77. Tianshu Yu, Runzhong Wang, Junchi Yan, Baoxin Li: Deep latent graph matching. In: Proceedings of the 38th International Conference on Machine Learning (2021)
78. Timothee Cour, Praveen Srinivasan, Jianbo Shi: Balanced graph matching. In: Advances in Neural Information Processing Systems 19 (2007)
79. Tjalling C Koopmans, Martin Beckmann: Assignment problems and the location of economic activities. *Econometrica* **25**(1), 53–76 (1957)
80. Utkarsh Gaur, Yingying Zhu, B. Song, Amit Roy-Chowdhury: A “string of feature graphs” model for recognition of complex activities in natural videos. In: IEEE International Conference on Computer Vision (2011)
81. Van den Bout, Miller, T.K.: Graph partitioning using annealed neural networks. *IEEE Transactions on Neural Networks* **1**(2), 192–203 (1990)
82. Weizhi Nie, Anan Liu, Yuting Su, Huanbo Luan, Zhaoxuan Yang, Liujuan Cao, Rongrong Ji: Single/cross-camera multiple-person tracking by graph matching. *Neurocomputing* **139**(2), 220–232 (2014)
83. William Brendel, Sinisa Todorovic: Learning spatio-temporal graphs of human activities. In: IEEE International Conference on Computer Vision (2011)
84. Wilson Richard, Hancock Edwin: Structural matching by discrete relaxation. *IEEE Transactions on Pattern Analysis Machine Intelligence* **19**(6), 634–648 (1997)
85. Yang Shen, Weiyao Lin, Junchi Yan, Mingliang Xu, Jianxin Wu, Jingdong Wang: Person re-identification with correspondence structure learning. In: IEEE International Conference on Computer Vision (2015)
86. Yue Wu, Zhenglei Xiao, Shaodi Liu, Qiguang Miao, Wenping Ma, Maoguo Gong, Fei Xie, Yang Zhang: A two-step method for remote sensing images registration based on local and global constraints. *IEEE Journal of Selected Topics in Applied Earth Observations and Remote Sensing* **14**, 5194–5206 (2021)
87. Yuille Alan, Rangarajan Anand: The concave-convex procedure. *Neural Comput.* **15**(4), 915–936 (2003)
88. Zhang, S., Liu, M., Yan, J., Zhang, H., Huang, L., Yang, X., Lu, P.: M-mix: Generating hard negatives via multi-sample mixing for contrastive learning. In: Proceedings of the 28th ACM SIGKDD Conference on Knowledge Discovery and Data Mining, pp. 2461–2470 (2022)
89. Zhen Zhang, Wee Sun Lee: Deep graphical feature learning for the feature matching problem. In: Proceedings of the IEEE Conference on Computer Vision and Pattern Recognition (2019)
90. Zhen Zhang, Yijian Xiang, Lingfei Wu, Bing Xue, Arye Nehorai: Kergm: Kernelized graph matching. In: Advances in Neural Information Processing Systems (2019)
91. Zhirong Wu, Shuran Song, Aditya Khosla, Fisher Yu, Linguang Zhang, Xiaoou Tang, Jianxiong Xiao: 3d shapenets: A deep representation for volumetric shapes. In: Proceedings of the IEEE Conference on Computer Vision and Pattern Recognition (2015)
92. Zhuang Liu, Mingjie Sun, Tinghui Zhou, Gao Huang, Trevor Darrell: Rethinking the value of network pruning. In: International Conference on Learning Representations (2019)